Marine Geology 377 (2016) 40–57

Contents lists available at ScienceDirect

Marine Geology

journal homepage: www.elsevier.com/locate/margo

Quaternary chronostratigraphic framework and sedimentary processes for the Gulf of Cadiz and Portuguese Contourite Depositional Systems derived from Natural Gamma Ray records

Johanna Lofi [a,*], Antje Helga Luise Voelker [b,c], Emmanuelle Ducassou [d], F. Javier Hernández-Molina [e], Francisco J. Sierro [f], André Bahr [g], Aurélie Galvani [h,a], Lucas J. Lourens [i], Eulogio Pardo-Igúzquiza [j], Philippe Pezard [a], Francisco Javier Rodríguez-Tovar [k], Trevor Williams [l]

[a] Géosciences Montpellier, Université de Montpellier, Place E. Bataillon, 34095 Montpellier, France
[b] IPMA, Divisão de Geologia e Georecursos Marinhos, 1449-006 Lisboa, Portugal
[c] CCMAR—Centro de Ciencias do Mar, Universidade do Algarve, Campus de Gambelas, 8005-139 Faro, Portugal
[d] Université de Bordeaux, UMR-CNRS 5805 EPOC, Allée Geoffroy St Hilaire, 33615 Pessac cedex, France
[e] Dept. Earth Sciences, Royal Holloway Univ. London, Egham, Surrey TW20 0EX, UK
[f] Geology Department, Salamanca University, Salamanca, Spain
[g] Institute of Earth Sciences, Heidelberg University, 69120 Heidelberg, Germany
[h] GDF SUEZ, La Défense, Paris, France
[i] Institute of Earth Sciences, Utrecht University, The Netherlands
[j] Geological Survey of Spain—IGME, 28003 Madrid, Spain
[k] Dept. Stratigraphy and Palaeontology, 18002 Granada, Spain
[l] International Ocean Discovery Program, Texas A&M University, College Station, USA

ARTICLE INFO

Article history:
Received 24 March 2015
Received in revised form 11 December 2015
Accepted 15 December 2015
Available online 17 December 2015

Keywords:
Gamma Ray
Contourites
MOW
Sea-level
Precession
Quaternary
Gulf of Cadiz

ABSTRACT

The Contourite Depositional Systems (CDS) in the Gulf of Cádiz and on the West Iberian margin preserve a unique archive of Mediterranean Outflow Water (MOW) variability over the past 5.3 Ma. These CDS have been recently drilled in several places during the IODP Expedition 339. These drill sites now offer a new window to the internal Pliocene and Quaternary architecture of the CDS. In this study, we use downhole and core Gamma Ray (GR) data acquired from 5 sites drilled in the CDS along the middle slope and 1 site drilled in the deeper setting of the lower slope, out of the MOW path. The GR data primarily tracks the clay content in the sediment and is the expression of sediment supply and, for sites drilled in the CDS, of the bottom current processes. Both appear astronomically controlled as shown by spectral analysis performed on the GR data. Results also reveal that the GR log patterns correlate well across the sites over the last 1.4 My. Several GR horizons corresponding to drops in GR values were identified, most of which fit with coarse-grained deposits observed in cores and interpreted as contourite beds. The GR horizons are interpreted as isochronous horizons, providing a regional scale chronostratigraphic framework for the CDS depositional records with an accuracy of ~20 ky. We further assess the spatial and temporal variability of the CDS hiatuses at the regional scale.

1. Introduction & geological background

Contourite Depositional Systems (CDS) generated by bottom current activity have been described on continental slopes, rises and abyssal plains (for a state of the art, see Rebesco et al., 2014). Beside a possible economic interest, CDS form sedimentary archives that are crucial for paleoceanographic and environmental (climate and sea-level) reconstructions. Among them, the CDS of the Gulf of Cádiz present an ideal contourite laboratory that has been studied for many years, mainly from shallow core data and seismic profile interpretation (e.g. Faugères et al., 1985; Nelson et al., 1999; Llave et al., 2001, 2007, 2011; Hanquiez et al., 2007; Hernández-Molina et al., 2003, 2006, 2014a; García et al., 2009; Marchès et al., 2007, 2010; Roque et al., 2012; Brackenridge et al., 2013). Moreover, in the framework of the Integrated Ocean Drilling Program (IODP), the Gulf of Cádiz CDS have been recently drilled in several places during Expedition (Exp.) 339 (Stow et al., 2013). These drill sites now offer a new window to the internal Pliocene and Quaternary architecture of the CDS, and thus the possibility to assess the spatial and temporal variability of the depositional records and hiatuses at the regional scale.

The Gulf of Cádiz is located westward of the Gibraltar Strait (Fig. 1), at the boundary between the Eurasian and African plates. It has a long and complex geological history dominated during the Plio-Quaternary

* Corresponding author.
E-mail address: johanna.lofi@gm.univ-montp2.fr (J. Lofi).

http://dx.doi.org/10.1016/j.margeo.2015.12.005
0025-3227/

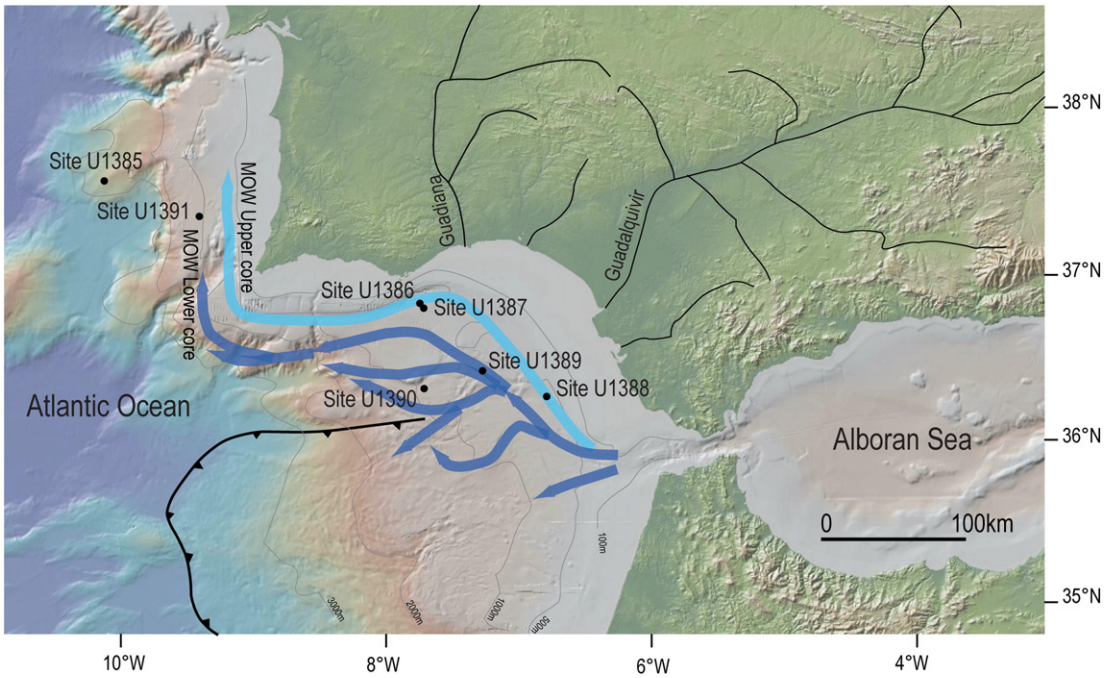

Fig. 1. Bathymetric map of the Gibraltar Strait area showing the location of the IODP Exp. 339 drilling sites. The main flow paths of the Mediterranean Outflow Waters (MOW) are indicated by the blue arrows (light blue: upper MOW core; dark blue: lower MOW core).
Modified from Stow et al. (2013).

by the development of extensive CDS generated by the influence of the Mediterranean Outflow Waters (MOW) emplaced after the opening of the Gibraltar Strait at 5.3 Ma (Stow et al., 2013; Hernández-Molina et al., 2014a, 2016). Preliminary results from Exp. 339 show that contourite deposition started from 4.2 to 4.5 Ma, increasing in the Quaternary (Stow et al., 2013, Fig. 2), but developed mainly during the last 2 Ma (Hernández-Molina et al., 2014b). Significant widespread unconformities, present in all CDS sites but with hiatuses of variable

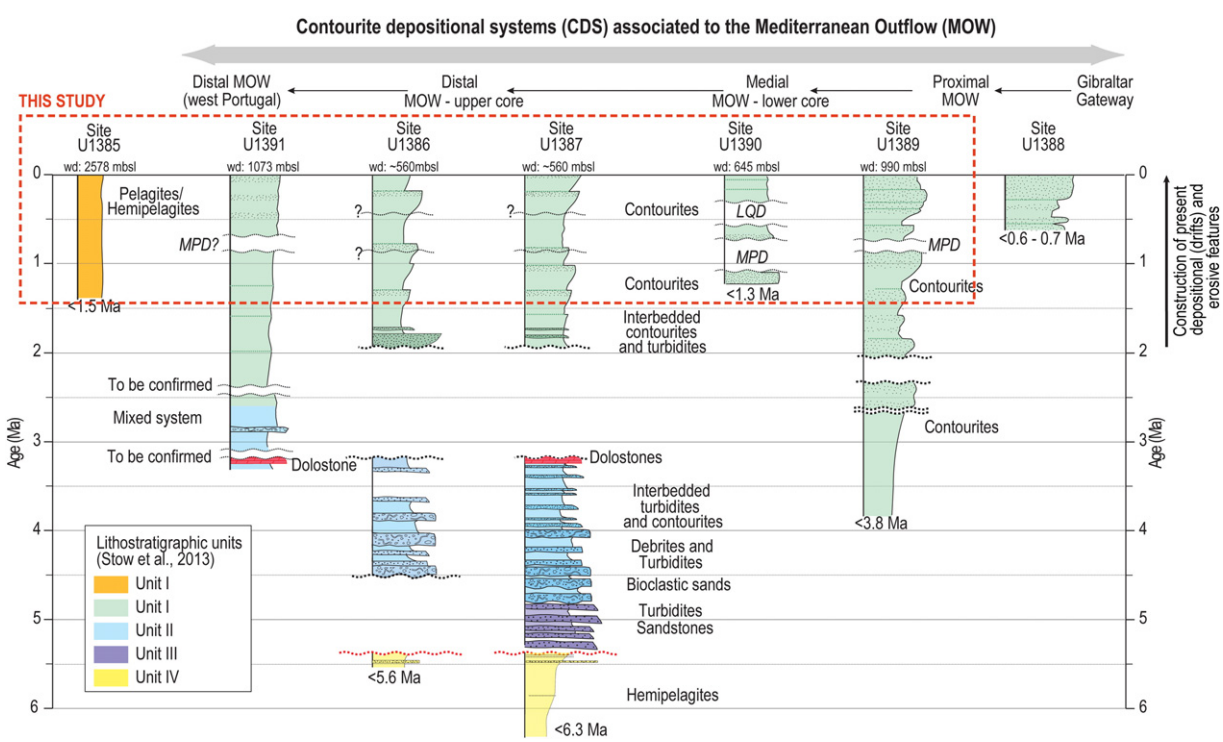

Fig. 2. Lithologic summary for sites drilled during IODP Exp. 339. The studied intervals cover the Pleistocene–Holocene sequence at 6 Sites (red square). Five of them are drilled in the CDS and consist of mainly contourite deposits. Site U1385, out of the CDS, consists of hemipelagic deposits. LQD: Late Quaternary discontinuity; MPD: mid-Pleistocene discontinuity; wd: water depth.
Modified from Hernández-Molina et al. (2006).

duration, are interpreted as a signal of intensified MOW, coupled with flow confinement (Llave et al., 2001, 2007, 2011; Marchès et al., 2007, 2010; Roque et al., 2012; Brackenridge et al., 2013). Among them, two major hiatuses at 3.2–3.0 Ma (Lower Pliocene Discontinuity, LPD) and 2.4–2 Ma (Early Quaternary Discontinuity, EQD) indicate erosion by bottom-currents and enhanced interaction between MOW and the North Atlantic (Hernández-Molina et al., 2014b). Another younger major regional discontinuity (Mid Pleistocene Discontinuity, MPD) with local erosion is clearly evident in the seismic records and is attributed to the mid-Pleistocene transition, with a preliminary tentative age of 0.9 Ma (Llave et al., 2004; Hernández-Molina et al., 2016). A pronounced change in the drift sedimentary stacking pattern appears at this time horizon as enhanced upslope progradation and mounded morphology indicating intensification of MOW. However, no clear hiatus or condensed section was found during the Exp. 339 in most of the drill core material at the 0.9–0.7 Ma time horizon (Stow et al., 2013).

The main sources of sediment supply to the Gulf of Cádiz are the Guadalquivir river to the East and the Guadiana to the North (Maldonado and Nelson, 1999; Fig. 1). Modern hydrography is dominated by exchange of water masses through the Gibraltar Strait. At the sea surface, the North Atlantic Surface Water (NASW) flows into the Mediterranean Sea. At depth, a deep undercurrent is formed by the highly saline MOW flowing out of the Mediterranean Sea (Baringer and Price, 1999). The MOW is mainly a mixture of the Levantine Intermediate Water (LIW) originating in the eastern Mediterranean, and the Western Mediterranean Deep Water (WMDW) formed in the Liguro-Provençal Basin and the Gulf of Lions. The LIW is estimated to contribute up to 90% of the MOW volume (Millot et al., 2006; Rogerson et al., 2012). After its passage through the Gibraltar Strait, the MOW flows westward and northwestward, following the contours of the Spanish and Portuguese continental slopes (Fig. 1). Its distribution is conditioned by the complex morphology of the slope, which generates two main cores (Borenäs et al., 2002; Serra et al., 2005): the upper core of the MOW, between 500 and 700 m below sea level (mbsl), and the lower core of the MOW, between 800 and 1400 mbsl. Below the MOW, the cold and less saline North Atlantic Deep Water (NADW) water mass flows at depths exceeding 1400 mbsl (van Aken, 2000).

The impact of the along-slope flow of the MOW on sedimentary processes along the Spanish and Portuguese continental slopes is evidenced by the presence of large contourite deposits (drifts). Contourite records have been recognized and described by many authors either from core data analysis or seismic profile interpretations and are classically interpreted as reflecting increase of MOW bottom current competency and velocity (e.g. Gonthier et al., 1984; Faugères et al., 1985; Stow et al., 1986; Sierro et al., 1999; Llave et al., 2001, 2006; Schönfeld et al., 2003; Voelker et al., 2006; Llave et al., 2006; Toucanne et al., 2007; Rogerson et al., 2012; Roque et al., 2012; Brackenridge et al., 2013). The periods of maximum MOW activity and associated development of coarse contourites, however, appear to vary from one area to another, and their link with global climate and sea level are still discussed, especially in periods older than the late Pleistocene. In order to account for this spatial and temporal variability, it has been proposed that the main flow alternated between the upper and lower cores of the MOW, depending on the climatic conditions (e.g. Schönfeld and Zahn, 2000; Llave et al., 2006). During glacial periods, the MOW was denser and flowing (about 700 m) deeper than today (Schönfeld and Zahn, 2000; Rogerson et al., 2005; Llave et al., 2006; Voelker et al., 2006), favoring the development of sandy contourites at intermediate depths on the continental slope. In the meantime, the upper branch of the MOW was weakened and dominated by fine-grained sedimentation on the middle slope. The deep settling of the glacial MOW is thought to have influenced the formation of the North Atlantic thermohaline circulation possibly indirectly impacting the formation of the NADW (Rogerson et al., 2005, 2012; Voelker et al., 2006; Khélifi et al., 2011, 2014). In an opposite way, at high sea-level, the density of the MOW was lower (Cacho et al., 2000), and the upper core of the MOW was the more active path, aiding the deposition of sandy contourites at shallower water depths on the continental slope (Llave et al., 2006). MOW variability has also been demonstrated at the millennial scale. At this scale, contourite deposition is associated with cool climatic periods during which MOW velocity was higher compared to warm climatic intervals (Cacho et al., 2000; Llave et al., 2006; Voelker et al., 2006; Toucanne et al., 2007). The above interpretations are mainly based on high-resolution seismic profile interpretation and on ^{14}C dated sediment core data covering the last 50 ky. IODP Exp. 339 drilling now allows the validity of these scenarios to be tested over the Quaternary sedimentary history (e.g. Voelker et al., 2015; Kaboth et al., 2016; Bahr et al., 2014, 2015).

Gamma Ray (GR) data can help to assess the temporal and regional scale variability of the sedimentary records forming the CDS. Nearly all rocks exhibit some natural gamma radioactivity and the amount depends on the concentration of potassium, thorium, and uranium (e.g. Ellis and Singer, 2007). In general, high values identify fine-grained deposits containing K-rich clay minerals and absorbed U and Th compounds, so that the GR data signal primarily tracks clay content. Quartz and calcite, containing no radioactive elements, are identified by low values. Thus GR logs can be interpreted in terms of the stratigraphy, lithology, and geochemical composition of the formation (e.g. Inwood et al., 2013). Moreover, when the GR data are acquired downhole, they are measured in situ and are continuous in depth. They are thus unaffected by inter-core gaps, low core recovery intervals or possible core expansion. Since the GR signal can be measured in boreholes and on cores, it allows core-log integration and joint interpretations.

In the Gulf of Cádiz, Quaternary deposits in the CDS are dominated by nannofossil mud, calcareous silty mud, and silty bioclastic sand lithologies and contain bi-gradational contourite depositional sequences (Stow et al., 2013) in which the coarser-grained intervals are classically interpreted as reflecting phases of current intensification (Gonthier et al., 1984; Faugères et al., 1984). Preliminary shipboard analysis from Exp. 339 showed that the GR signal reflects this lithological variability (Stow et al., 2013). In the present study, we analyze core and downhole GR data from 6 sites drilled during Exp. 339 in order to investigate how the GR signal responds to change in lithology and associated paleo-environments. We also aim to correlate and track the Pleistocene deposits and contourite beds at the regional scale in order to reconstruct their spatial variability and test the existing scenario of enhanced MOW during cold climatic conditions.

2. Data and methods

2.1. Drilling sites

During IODP Exp. 339, from November 2011 to January 2012, five sites were drilled in the Gulf of Cádiz (U1386, U1387, U1388, U1389, and U1390) and two sites (U1385, U1391) off the West Iberian margin (Fig. 1). A detailed description of the drilled sites and drilling, coring, and logging operations is given in Stow et al. (2013). Age data were essential for determining the ages of key horizons (including several depositional hiatuses and stratigraphic boundaries) and the sedimentary accumulation rates (for updated chronology details about the IODP Sites see Table S1 in Hernández-Molina et al., 2014b).

Sites U1386 to U1391 were drilled to examine the influence of the MOW on CDS development (Figs. 1 and 2). Sites U1386 and 1387 were retrieved from the middle-slope Faro-drift, at water depths of 562 and 559 mbsl, respectively. Site U1388 was drilled in a sandy sheeted drift located in the proximal zone of the CDS, closest to the Strait of Gibraltar. Due to the low core recovery and of the absence of downhole logs at this site, Site U1388 has not been included in this study. Site U1389 (water depth ~645 mbsl) was drilled in the central area of the middle slope, between Cádiz and Faro, in order to recover sheeted and buried mounded drift successions. Site U1390 (993 mbsl)

penetrated a large sheeted drift located southeast of the Guadalquivir Bank, in an area affected by recent tectonic activity (Stow et al., 2013). Site U1391 (1073 mbsf) is the most distal site within the CDS and targeted a large plastered drift on the middle slope of the West Iberian (Sines) margin. Sites U1386, U1387, and U1388, are currently under the influence of the upper MOW core, whereas Sites U1389, 1390 and U1391 are affected by the lower MOW core.

Site U1385 is the only site that has been drilled in a deeper setting, below and to the west of the MOW path. This site is located on the West Iberian margin, at a water depth of 2578 mbsl, and offers a hemipelagic record over the last 1.43 Ma (Hodell et al., 2013, 2015). Site U1385 is currently under the influence of the Northeast Atlantic Deep Water (NEADW) and was bathed by southern sourced waters during glacial periods (Skinner and Elderfield, 2007; Margari et al., 2010).

2.2. HNGS downhole logs and NGR core logs

Downhole logs were acquired with Schlumberger logging tools at five sites (Holes U1386C, U1387C, U1389A, U1389E and U1391C), after completion of coring operations (Stow et al., 2013). The log data are continuous with depth and measured in situ. During rough seas, a wireline heave compensator system was used to compensate for the vertical up and down motion of the ship, maintaining a steady motion of the logging tools (Itturino et al., 2013) and reducing the possibility of depth discrepancies in the logging data. Where core recovery is incomplete or disturbed, logging data may provide the only way to characterize the borehole section (e.g. Ducassou et al., 2016). Downhole log data also allow the site lithostratigraphy to be linked to the seismic profiles using checkshot surveys and velocity logs (e.g. Hernández-Molina et al., 2016). Among the tools used during IODP Exp. 339, the Hostile Environment Natural Gamma Ray Sonde (HNGS) measured the natural gamma radiation (HSGR, standard total Gamma Ray) of the formation surrounding the boreholes (Serra, 1984). HSGR logs were acquired at a sampling interval of 15.24 cm (6 in.) and with an approximate vertical resolution of 20–30 cm. HSGR logs are expressed in meters wireline log depth below seafloor (mwsf). The HSGR signal is attenuated by the drill pipe, present in the upper 80–100 m of the Exp. 339 boreholes, but this attenuation can be partly corrected and the data presented here are normalized to the equivalent open-hole values (Stow et al., 2013).

A set of shipboard petrophysical measurements has also been performed on whole-round core sections. Among them, natural gamma radiation (NGR) core logs were acquired with a Natural Gamma Radiation Logger (NGRL) with a total of 8 measurements per 150 cm section (Stow et al., 2013). HNGS logs and NGR core data thus complement one another and where core recovery is good, allow core-log integration (e.g. Ducassou et al., 2016). In this study, both data sets (NGR and HSGR) have been interpreted jointly at each site. NGR logs are also expressed in meters below sea floor (mbsf), but since this depth scale is based on coring and curatorial procedures, a slight vertical offset, generally below 1 m, is often observed between core log data (in mbsf) and downhole log data (in mwsf) (Stow et al., 2013). The HNGS signal can also be correlated to the shipboard composite spliced NGR, which represents a more continuous record of the drilled formation, less affected by inter-core gaps. However, the depth scale of spliced records is expanded by about 10–11% because of core expansion on removal of in-situ pressures (Stow et al., 2013). Due to the very linear nature of the expansion, and in order to facilitate a direct comparison of the NGR spliced records with the HNGR (in mwsf) or NGR data (in mbsf), the splice records need to be compressed to produce a modified scale (called mbsf* in this paper) that approaches the original mbsf scale. For this purpose we applied the expansion factors that were established by the stratigraphic correlators during the offshore phase of Exp. 339 (Stow et al., 2013).

At a larger scale, an across site correlation of the GR logs acquired within the CDS has been performed using the software AnalySeries (Paillard et al., 1996). This correlation is based on the comparison of the GR log patterns over an interval covering the last ~1.45 Ma. We identified 49 “Gamma Ray horizons” (GRH; the lowest GR value observed over a section of log) corresponding to relatively well expressed drops to lower GR values that can be traced from site to site at the regional scale. The HSGR logs have been primarily used for this purpose because these downhole log data are continuous in depth and unaffected by inter-core gaps and low core recovery intervals. When downhole log patterns were not clear, correlations have been complemented by using the NGR and spliced NGR core log patterns. For Site U1385, no downhole logs were acquired and the revised spliced NGR core data (Hodell et al., 2015) have been used for comparison with the HSGR logs acquired at the other drilling sites.

2.3. Depth to time conversion

For the sites drilled in the CDS, we used the age models provided from recently published studies for Site U1387 (Table 1) and which are based on correlating XRF-derived or benthic foraminifer $\delta^{18}O$ records to regional or global standard chronologies (Bahr et al., 2014; Voelker et al., 2014, 2015; Singh et al., 2015). This provided a reliable timescale to date the 49 GRH previously identified at the regional scale. In the 217–662 ky interval, along which no age control points were available at Site U1387, the age model has been extrapolated assuming a constant sedimentation rate. We further used available age control points at different sites in order to test the proposed regional scale correlation and discuss the synchronicity of the GRH. These points, provided from recently published studies, mainly cover the topmost part of the Sites (Table 1).At the time this study has been performed, no age control points were available for Site U1391, and only few of them for Sites U1386 (Kaboth et al., 2016; Bahr et al., 2015), U1389 (Bahr et al., 2015) and U1390 (Voelker, personal communication). Shipboard biostratigraphic datums (Stow et al., 2013) have also been used for depth to time conversions. However, since the bio-events were primarily based on shipboard core catcher sample analysis (one sample every ~9.5 m), this chronostratigraphy is low resolution and may be subject to future revisions; so it has been of limited utility. In order to fully support the correlation presented in this study, some

Table 1
Age control points used in this study.

Site	Depth interval (mcd)	Age range (ky)	Authors	Method
U1385	0–166	0–1427	Hodell et al. (2015)	Benthic oxygen isotope record and correlation with LR04
U1386	0–48	0–150	Kaboth et al. (2016)	Benthic oxygen isotope record and XRF data
U1387	0–35	0–143	Bahr et al. (2014)	Tuning XRF Br counts on planktonic $\delta^{18}O$ of MD01-2444 using the Stratigraphy of Hodell et al. (2013)
	33–51	0–217	Singh et al. (2015)	Benthic oxygen isotope stratigraphy and correlation with LR04
	172–311	662–1188	Voelker et al. (2014, 2015)	Foraminiferal oxygen isotope record tuned to Lisiecki and Raymo (2005)
	158–386	620–1467	Bahr et al. (2015)	Lisiecki and Raymo (2005)
U1389	0–72	0–143	Bahr et al. (2015)	Tuning XRF-Br data on planktonic $\delta^{18}O$ of MD01-2444
U1390	103–137	81–136	Voelker A. (personal communication)	Benthic oxygen isotope record tuned to MD95-2042

additional independent age control points would be required along the intervals in which chronostratigraphic data are lacking.

For Site U1385 drilled in a deeper setting, we used the age model developed for the revised shipboard NGR splice (depth scale in rmcd), which is based on the benthic oxygen isotope record (Hodell et al., 2015). This provides an excellent timescale, accurate to within a few ky, to date records deposited out of the MOW path.

2.4. Lithological logs and sedimentological analyses

Since the GR signal primarily tracks the clay content of the formations, the NGR and HSGR logs were compared with the lithological logs drawn during the expedition based on visual core descriptions (VCD). This was supplemented by grain size analysis locally performed on core samples from Site U1387 from 40 to 350 mbsf. For the upper part of the holes (40–170 mbsf), grain-size has been measured with a laser microgranulometer MALVERN MASTERSIZER S (University of Bordeaux, EPOC laboratory). Sand, silt and clay fractions (>63 μm, 63–7 μm and <7 μm, respectively) are shown for this interval (2–50 cm resolution). For the lower part of the holes (170–350 mbsf), additional information (8–14 cm resolution) is provided by the weight percent (wt.%) of the sand fraction >63 μm that was calculated for the washed sediment samples (Bahr et al., 2014; Voelker et al., 2015). For the same depth interval the carbonate content was measured in discrete sediment samples using a LECO element analyzer (see Voelker et al., 2015 for details). We note that the grain-size and carbonate data are discontinuous in each hole, because they were acquired on samples taken from the composite splice section. The grain-size spliced records (in mcd, meters composite depth) can, however, be compared to the GR logs in mbsf or mwsf, by converting them from mcd into mbsf* depth scale (see above).

2.5. Spectral analysis

Spectral analysis is a well-known method for detecting periodicities embedded in noise. Here we used the Lomb–Scargle periodogram method, because it can be applied to irregularly sampled time series (Lomb, 1976; Scargle, 1982; Press et al., 1992; Pardo-Igúzquiza and Rodríguez-Tovar, 2012). This methodology has been successfully applied to paleoclimate and paleoceanographic time series with uneven sampling, even when dealing with short time series or with incidence by punctual events (Jiménez-Moreno et al., 2007; Rodríguez-Tovar et al., 2010; Pardo-Igúzquiza and Rodríguez-Tovar, 2012; Jiménez-Espejo et al., 2014).

In the present study, the Lomb–Scargle periodogram has been applied to the normalized HSGR data at 4 sites (U1386C, U1387C, U1389E, and U1391C; U1390 not included due to the presence of two hiatuses) in order to trace the record of orbital-scale variations in the sediment properties of the CDS over the last ~1.4 Ma. We used a sampling of 2000 frequencies between 0 and 1 cycle per ky. The significance level of the obtained spectral peaks was calculated by a Monte Carlo procedure, the so-called permutation test (e.g. Pardo-Igúzquiza and Rodríguez-Tovar, 2000, 2012 for a detailed description). This provides a non-parametric assessment of the statistical significance of the peaks in the power spectrum, that is, the probability of that peak having not being generated by pure chance. 2000 random permutations were used in this study, and a 100% confidence level for a given frequency was assigned if in none of the 2000 permutations there has been an amplitude spectrum that is larger than the one calculated with the original time series. On this basis, we only consider the most significant peaks, close to a 100% confidence level. The peaks registered in the lower frequency band close to the y-axis have not been taken into consideration because they could be affected by long-term trends in the data. We focused on the Milankovitch-band cyclicity, but the resolution of the records also permit sub-Milankovitch scale cycles to be examined.

3. Results

3.1. Core log integration

At sites drilled in the CDS (U1386 to U1391, excluding U1388), the Pleistocene–Holocene sequence forms the Unit I of Stow et al. (2013) (green unit in Fig. 2). This unit is dominated by nannofossil mud, calcareous silty mud, and silty bioclastic sand lithologies (Table 2). These lithologies generally organize as bi-gradational sequences (contourites), the most complete of which coarsen upward from nannofossil muds to calcareous silty muds to silty bioclastic sands, and then fine upward through calcareous silty mud into nannofossil mud, with a predominance of gradational contacts and extensive bioturbation. These sequences are classic contourite deposition accumulated under the action of bottom current processes (Gonthier et al., 1984). Partial sequences are also common and occasional turbidite intercalations with normally graded sequences occur in several sites. As a result, some of the contourite muds retain a distinctive lamination, albeit discontinuous in character, whereas the sands are especially clean and well sorted.

3.1.1. Core scale

The Gamma Ray signal primarily tracks the clay content in the sediment. For the lithologies forming Unit 1 in the CDS (Table 2), the GR signal also depends on the $CaCO_3$ content, which dilutes the clay content, and of the grain size, because quartz-rich sand and silt similarly dilutes the clay content. A comparison between lithology, sand fraction and NGR core data over a 10 m long interval from Hole U1387B (252–262 mbsf; core 28X) is given in Fig. 3 as an example. At the scale of the core, the NGR signal trend mirrors the clay content and is inversely correlated to the amount of $CaCO_3$ in the sediment. Relatively high NGR values (>40–45 cps) are observed when the carbonate content is below

Table 2
Main lithologies forming the Pleistocene–Holocene interval at the IODP EXP. 339 studied sites. Compilation based on the shipboard descriptions (Stow et al., 2013).

Site	Lithologic units	Depth (mbsf)	Age	Main lithology
U1385	Unit I	0–152	Holocene–Pleistocene	Bioturbated nannofossil muds and nannofossil clays. Hemipelagic succession.
U1386	Subunit IA	0–110	Holocene–Pleistocene	Nannofossil mud, calcareous silty mud, and silty sand with biogenic carbonate. Mixed sandy and muddy contourite succession.
	Subunit IB	110–215	Pleistocene	Nannofossil mud and calcareous silty mud. Reduced abundance of coarser grained lithologies compared to subunit IA. Muddy/silty contourite succession.
	Subunit IC	215–420	Pleistocene	Nannofossil mud, calcareous silty mud, and silty sand with biogenic carbonate. Mixed sandy and muddy contourite succession with increased abundance of coarser lithologies downhole and appearance of silty turbidites in the lowermost 30 m.
U1387	Unit I	0–454	Holocene–Pleistocene	Nannofossil mud, silty mud with biogenic carbonate, and silty sand with biogenic carbonate. Mixed sandy/muddy contourite succession with few turbidites.
U1389	Subunit IA	0–310	Holocene–Pleistocene	Calcareous mud (63%), silty and sandy mud with biogenic carbonate. Little evidence of a direct turbidity current input. Contourite-dominated depositional system.
	Subunit IB	310–387	Pleistocene	Calcareous mud (82%), silty and sandy mud with biogenic carbonate. Coarser grained lithologies in non recovered intervals? Contourite-dominated depositional system.

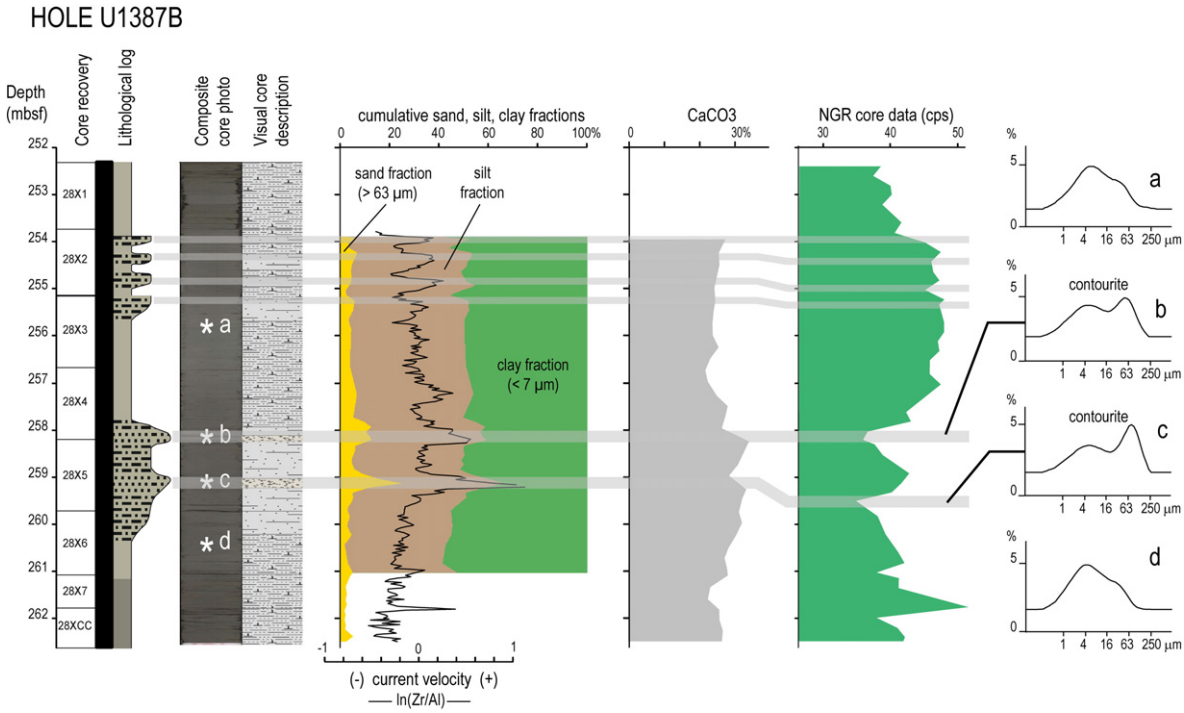

Fig. 3. Core log integration over a 10 m long interval in Hole U1387C. The data set includes the lithological log, composite core photos, visual core description, clay, silt and sand fractions, $CaCO_3$ content, and NGR data acquired on whole round cores. To the right, grain-size results are shown for two samples taken in the sandy contourite beds (b and c) and two samples taken out of them. See asterisks on composite photo for sample location. The Zr/Al ratio XRF data (Voelker et al., 2015) represents the relative enrichment of heavy minerals (zircon) over less dense aluminosilicates under current flow, and is used as a semi-quantitative indicator of current velocity (Bahr et al., 2014).

20%, and vice versa. This is in agreement with the absence of radioactive minerals in carbonate, when they are abundant in clays. Superimposed on the NGR trend, we observe several more or less well expressed drops to lower NGR values (e.g. ~258 and 259 mbsf). These drops correlate in cores with coarse-grained intervals corresponding to mixed sandy and muddy contourite deposits, clearly shown by an increase in the sand fraction (or wt.% of the sand fraction) and a decrease in clay fraction content (Fig. 3). The Zr/Al ratio represents the relative enrichment of heavy minerals (zircon) over less dense aluminosilicates under current flow, and is used as a semi-quantitative indicator of current velocity (Bahr et al., 2014). In Fig. 3, the ln(Zr/Al) data mirror the mean grain size. The acoustic velocity peaks coincide well with sand peaks, i.e. the sandiest part of the respective contourite layer.

3.1.2. Borehole scale

A similar relationship can be observed at the borehole scale. Fig. 4 illustrates the upper 350 m of Site U1387 in which the good core recovery allows core/log integration. NGR core data from Holes A, B and C and spliced NGR core data can thus be compared with the downhole HSGR log acquired in open Hole C. The HSGR curve correlates well with the NGR curves from the 3 holes and from the splice, as highlighted by the gray lines (GRH that can be traced at the regional scale). Small depth offsets (generally less than a few meters) are observed locally, probably due to discrepancies in the depth scales (core mbsf for Holes A to C, mbsf* for the splice, and mwsf for the downhole logs; see Stow et al., 2013 for details), gaps between two successive cores, and/or possible core gas expansion, especially in clay rich intervals.

The NGR and HSGR logs of Site U1387 are characterized by medium-amplitude cyclic swings, varying on a decimeter to submeter scale, with no major steps in the base levels. These medium-amplitude swings are generally well anti-correlated with the $CaCO_3$ content in the sediments (see spliced data in Fig. 4), suggesting that the GR signal is at low frequency the expression of clay dilution by carbonate (or inversely). Superimposed on these swings, relatively thin GR excursions toward lower values (black arrows in Fig. 4) generally fit well with coarse-grained intervals, evidenced by sand peaks and in most cases showing a bi-gradational trend. Generally, the sandier the deposit is, the stronger the GR drop is (e.g. Hole A, Cores 35X and 36X). These deposits are also associated with higher carbonate content (see spliced data in Fig. 4; e.g. Voelker et al., 2015; Lebreiro et al., 2015). A few coarse-grained intervals fit with a peak in GR counts (orange arrows in Fig. 4). This is for example clearly observed from core data in Hole A, Core 21X and Hole B, Core 23X. Some decreases in GR counts also do not correlate with obvious changes in the lithological logs (blue arrows in Fig. 4). However, in such cases, the drop in GR generally remains of modest amplitude.

3.2. Regional scale correlation and sedimentation rates

At the regional scale, 49 GRH have been identified in the CDS and labeled GRH 1 to GRH 49, from top (sea floor) to bottom (Table 3). These GRH are more or less pronounced and well expressed troughs (relatively low values) in the GR logs (Fig. 4) and can be confidently traced across the 5 studied sites (U1391, U1386, U1387, U1389, and U1390). Fig. 5 illustrates the proposed regional scale correlation against time, i.e. for the past ~1.45 Ma, based on the age models of Site U1387. The GR logs are also plotted against the revised splice NGR core data of Site U1385 (Hodell et al., 2015), which has its own age model and provides a record out of the MOW path. The GR logs are also plotted against the LR04 stack curve of Lisiecki and Raymo (2005), which is a globally distributed benthic $\delta^{18}O$ stacked record reflecting global ice volume and deep ocean temperature. Fig. 5 clearly shows that the general trends of the GR curves correlate well across the sites drilled in the CDS, and also extend to Site U1385. There is a strong similitude in the log patterns across most of the studied intervals at all Sites (e.g. GRH 5 to GRH 34). The topmost part (above GRH 5) and the bottom part of the holes (below GRH 34), however, show less clear patterns, at least for some of the Sites. The characteristics of each site are presented below.

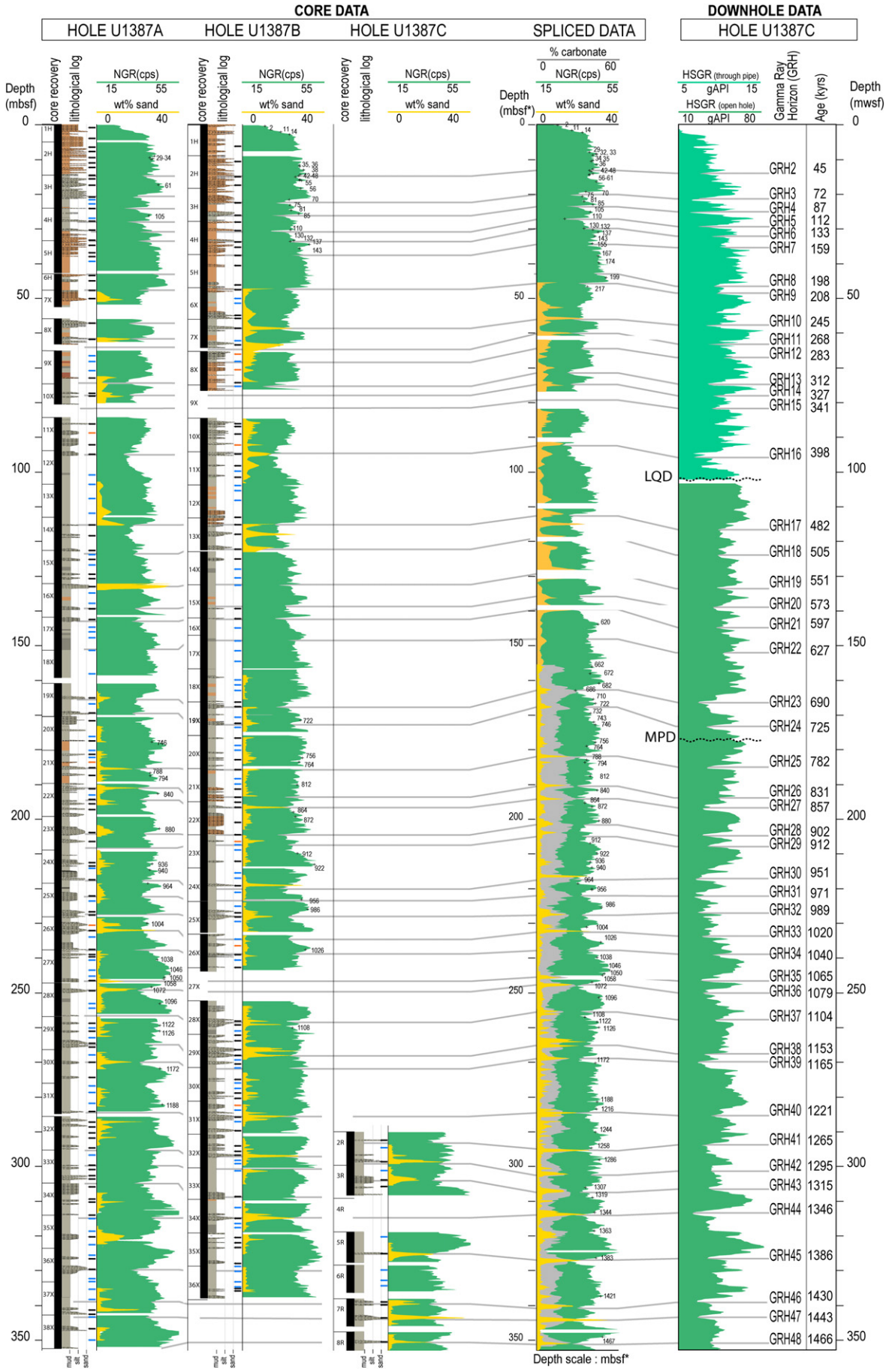
CORE DATA
HOLE U1387A
HOLE U1387B
HOLE U1387C
SPLICED DATA
DOWNHOLE DATA
HOLE U1387C
Depth (mbsf)
core recovery
lithological log
NGR(cps)
wt% sand
% carbonate
Depth (mbsf*)
HSGR (through pipe)
HSGR (open hole)
Gamma Ray Horizon (GRH)
Age (kyrs)
Depth (mwsf)
LQD
MPD
Depth scale : mbsf*

Table 3
Depth and age the Gamma Ray (GR) horizons (trough correlating with contourite beds in the CDS) that can be traced across Sites U1391, U1386, U1387, U1389 and U1390. Site U1387 has been used as reference age model. In the 217–662 ky interval along which no age control points were available at Site U1387 (Table 1), the age model has been extrapolated assuming a constant sedimentation rate. Horizontal lines indicate the main Gamma Ray horizons (GRH) horizons identified at the regional scale and plotted in Figs. 4, 5 and 6.

GR horizon	Age (in ky) tuned to Site U1387	U1391C	U1386C	U1387C	U1389E	U1390A
		HSGR depth (mwsf)	HSGR depth (mwsf)	HSGR depth (mwsf)	HSGR depth (mwsf)	HSGR depth (mwsf)
GRH1	0	0.0	0.0	0.0	0.0	0.0
GRH2	45	20.3	18.9	14.1	24.9	52.4
GRH3	72	24.4	25.8	21.8	38.8	84.3
GRH4	87	29.2	29.7	25.2	49.5	99.8
GRH5	112	33.7	37.6	29.3	56.6	115.5
GRH6	133	39.2	43.2	32.1	61.1	120.6
GRH7	159	44.6	47.5	35.2	64.3	133.7
GRH8	198	54.6	60.9	46.4	79.3	153.8
GRH9	208	57	63.8	48.6	81.4	161.2
GRH10	245	64.4	75.1	57.9	95.7	185.7
GRH11	267	68.2	81.8	63.4	104.7	194.7
GRH12	283	77.9	86.6	67.4	112.3	H
GRH13	312	84	95.2	74.5	126.4	H
GRH14	327	88.3	100.5	78.0	136.4	H
GRH15	341	93.6	104.6	81.6	143.6	H
GRH16	398	108.7	123.7	95.6	168.5	H
GRH17	482	117.7	147.5	116.5	222.1	H
GRH18	505	125	155.6	122.2	229.4	H
GRH19	551	133.7	170.3	133.6	250.9	H
GRH20	573	138.8	178.7	138.8	259.8	H
GRH21	597	142	185.5	145.0	265.6	H
GRH22	627	148.8	197.7	152.4	275.9	H
GRH23	690	161.3	213.9	166.4	301.4	H
GRH24	725	174	225.6	173.5	317.6	225.9
GRH25	782	187.4	242.4	185.2	H	243.9
GRH26	831	200.5	253.4	192.6	H	H
GRH27	857	207.2	259.6	197.7	H	H
GRH28	902	229	275.1	204.6	H	H
GRH29	912	232	279.2	207.8	H	H
GRH30	951	246.6	298.0	217.3	H	H
GRH31	971	254.6	307.2	222.4	H	H
GRH32	989	260.3	316.5	226.9	H	H
GRH33	1020	271.5	331.6	233.8	H	H
GRH34	1040	275.1	348.2	239.0	H	H
GRH35	1065	282.8	362.1	246.1	H	H
GRH36	1079	288.1	368.8	250.1	H	H
GRH37	1104	297.5	387.8	258.0	326.3	H
GRH38	1153	313.3		267.7	347.4	H
GRH39	1165	316.2	406.4	270.1	353.2	263.3
GRH40	1221	333.4	425.6	285.4	382.5	282.7
GRH41	1265	347.4	439.5	293.9	384.9	293.5
GRH42	1295			278.4		302.6
GRH43	1315			306.2		
GRH44	1346	367.7	462.9	313.5	417.5	
GRH45	1386		474.9	326.4		330.1
GRH46	1430	389.3	487.5	338.9	438.7	
GRH47	1443	392.2		343.5	441.2	
GRH48	1466		497.9	351.0	447.6	
GRH49	1495	405.9		360.7	455.5	

The HSGR log in Hole U1391C correlates well with the logs of Sites U1386, U1387 and U1389, as well as with the spliced NGR of Site U1385. A strong similarity is observed in the log patterns (Fig. 5). The mean sedimentation rates vary from 21 cm/ky to 31 cm/ky over the studied interval (Fig. 7A), which is in agreement with the shipboard estimate (27 cm/ky, Stow et al., 2013). A small anomaly is observed between 398 and 482 ka (108–117 mbsf), associated with a change in the sedimentation rate, suggesting the presence of a hiatus of short duration, falling somewhere between Marine Isotope Stages (MIS) 11 and 13 (Fig. 5). At Site U1385, the early part of MIS 11 is marked by a very low sedimentation rate (condensed section) (Hodell et al., 2015) and could correlate laterally with this hiatus. Moreover, this hiatus would fit laterally in depth with a regional seismic unconformity (Late Quaternary Discontinuity, LQD) observed in the same interval (early MIS 11) at Site U1387C (Fig. 5, Hernández-Molina et al., 2016), and predicted with multichannel seismic data at Site U1391, a few tens of meters shallower (~GRH 15, Fig. 5). A very low sedimentation rate in this 108–117 mbsf interval is, however, not excluded. Another seismic unconformity (MPD) is observed deeper at Site U1391, at ~200 mbsf (~GRH 26, Fig. 5) (Hernández-Molina et al., 2016), suggesting the possible existence of another hiatus. A hiatus is not supported by the HSGR logs, which correlate closely along this interval with the spliced NGR at Site U1385 (Fig. 5), however a change in the sedimentation rate is however observed between 200 and 207 mbsf (~831–857 ka, GRH 26-27, Fig. 7-A), falling somewhere between MIS 20 and 21 (Fig. 5). This interval coincides at this site with the predicted depth of the MPD with multichannel seismic data (Fig. 5; Hernández-Molina et al., 2016) and could represent a conformable contact, which grades laterally into the discontinuity.

Site U1387 is the best constrained in terms of age control points (Table 1, Figs. 5, 6). The HSGR log in Hole U1387C correlates relatively well over the entire interval with the logs acquired at the other Sites. Two main seismic unconformities have been observed at Site U1387 (LQD and MPD, Fig. 5). The estimated depth of the LQD unconformity roughly coincides with MIS 11 and the one of the MPD falls somewhere between MIS 24 and 25 (Figs. 5, 6). The HSGR log does not give any evidence that these unconformities could correspond to hiatuses in the sedimentary record at the site position (Fig. 5), which for the MPD is conform to the existing paleoclimate records (Voelker et al., 2014). The mean sedimentation rate at Site U1387 is relatively uniform at approximately 23 cm/ky (Fig. 7-C), in agreement with the shipboard estimate (25 cm/ky).

The log patterns of Sites U1386 and U1387 correlate very well above GRH 38 (Fig. 5), which is consistent with the proximity of the two sites to each other, both drilled into the Faro drift. In the topmost 30 m (above GRH 4), the pattern of Hole U1386C, however, presents an anomaly characterized by a bigradational shape with a maximum GR value centered around ~15 mbsf (last ~50 ky) (Fig. 5). This pattern cannot be correlated with the other sites and is likely due to an acquisition artifact, possibly related to anomalies in the steel pipe. Indeed, the NGR core data at this site do not show this bigradational shape (Stow et al., 2013) and its pattern is very consistent with the ones observed at both Sites U1391 and U1387. The HSGR in this interval has consequently not been used for correlation purpose. A mean sedimentation rate of ~34 cm/ky is estimated in Hole U1386C, in agreement with the shipboard estimates (35 cm/ky). Two changes in the sedimentation rate are observed, at ~307 (GRH 31) and ~387 mbsf (GRH 37) (Figs. 5, 7-B). Two seismic unconformities were recognized at this site, at ~112 and 316 mbsf, corresponding to the LQD and MPD, respectively (Hernández-Molina et al., 2016). We have no evidence for the shallowest one in our HSGR data. The deepest unconformity falls in the 307–387 mbsf interval in which the sedimentation rate reaches 56 cm/ky. This increase in sedimentation rate is in agreement with the geometries observed on the seismic profiles, above and below the MPD unconformity (Hernández-Molina et al., 2016). However, we cannot exclude

Fig. 4. Core log shipboard data integration at Site U1387 illustrating the correlation between the lithological logs, sand fractions, NGR (natural gamma radiation) core data acquired on whole round cores (Holes U1387A, U1387B and U1387C), spliced NGR core data (Stow et al., 2013), spliced sand fraction and carbonate content, and the HSGR (standard total Gamma Ray) data acquired in open hole U1387C. Black arrows: coarse grained intervals correlating with GR low values; orange arrows: coarse-grained intervals correlating with GR peaks; blue arrows: decrease in the GR counts correlating with nothing obvious in the lithological logs; LQD (Late Quaternary discontinuity) and MPD (mid-Pleistocene discontinuity) predicted depths (Hernández-Molina et al., 2016). Gray lines indicate the main Gamma Ray horizons (GRH) identified at the regional scale.

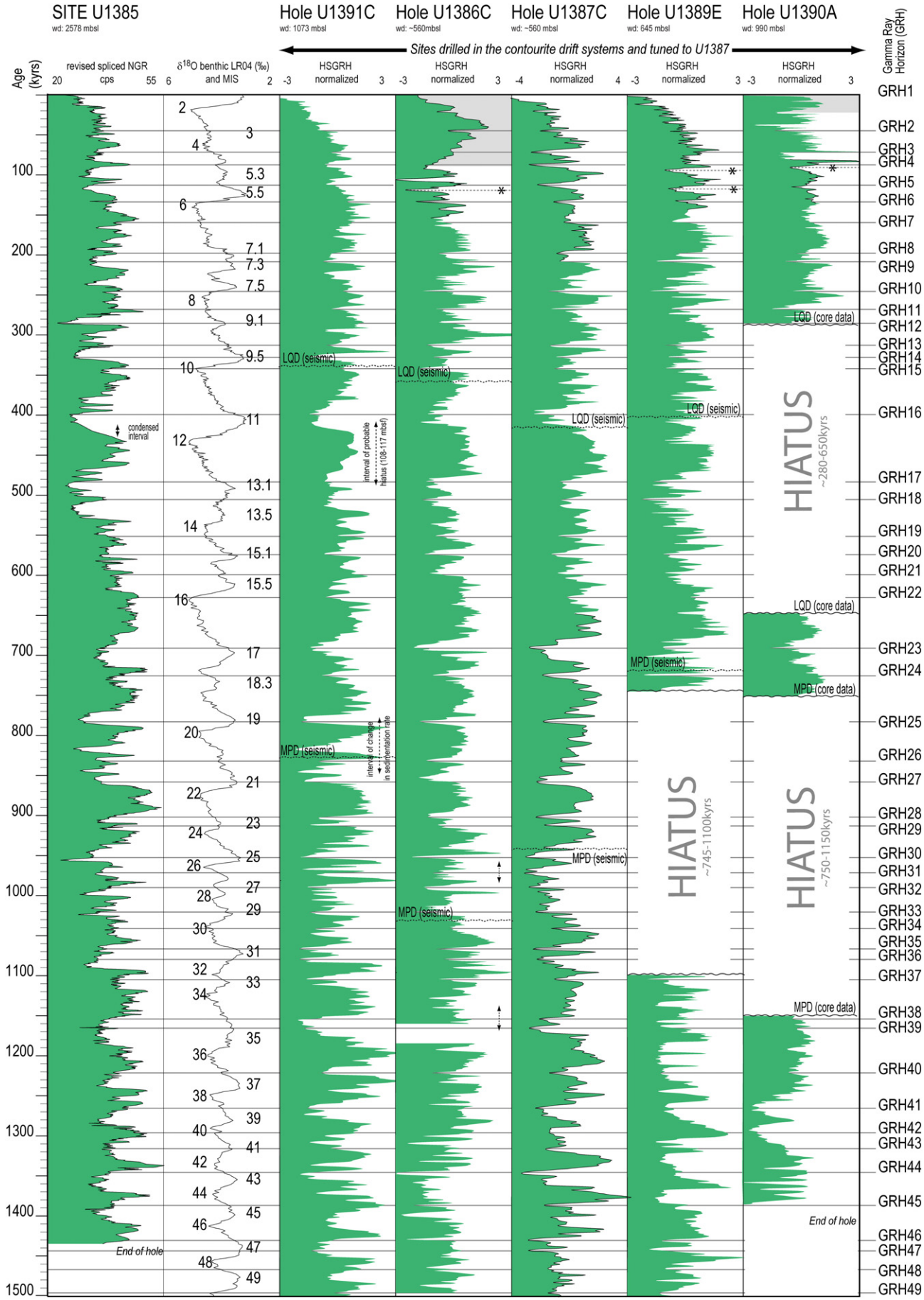
SITE U1385
wd: 2578 mbsl
Hole U1391C
wd: 1073 mbsl
Hole U1386C
wd: ~560mbsl
Hole U1387C
wd: ~560 mbsl
Hole U1389E
wd: 645 mbsl
Hole U1390A
wd: 990 mbsl
Sites drilled in the contourite drift systems and tuned to U1387
Age (kyrs)
revised spliced NGR
cps
δ18O benthic LR04 (‰) and MIS
HSGRH normalized
Gamma Ray Horizon (GRH)
condensed interval
LQD (seismic)
MPD (seismic)
interval of probable hiatus (108-117 mbsf)
interval of change in sedimentation rate
LQD (core data)
MPD (core data)
HIATUS
~280-650kyrs
~745-1100kyrs
~750-1150kyrs
End of hole

that the change observed beneath 387 mbsf is related to correlation issues, since the log pattern becomes less clear beneath ~GRH 34 (Fig. 5) possibly as a result of an increase in turbidite content below 370 mbsf, as reported by Alonso et al. (2016) for the early Pleistocene. The turbidites become even more abundant below ~420 mbsf (unit II in Stow et al., 2013). In the proposed correlation, the biozones are not always in agreement with the proposed age model, which may be explained by reworking in the turbidite-rich interval.

The HSGR log in Hole U1389E correlates well with the sites previously described, down to GRH 24, and with more caution down to GRH 49. Based on the log correlation patterns and the last occurrence (LO) of *Reticulofenestra asanoi* (0.90 Ma) placed between 322 and 332 mbsf during Exp. 339, we suggest the existence of a hiatus at ~326 mbsf. Its duration would not exceed 400 ky (745–1110 ka). In this interpretation, the disappearance of *R. asanoi* would thus be related to erosion associated to the hiatus. The relatively regular sedimentation rates above and below 326 mbsf (44 cm/ky and 32 cm/ky, respectively, Fig. 7D) supports this interpretation. In addition, the MPD seismic unconformity has been observed at this site at a predicted depth of ~320 mbsf, which is very close to the depth at which we place this hiatus (Fig. 5).

The HSGR log pattern from Hole U1390A is less clear than at the other sites due to the presence of two hiatuses. Its lateral correlation at the regional scale remains subject to caution. The two hiatuses identified at this site on the basis of the shipboard micropaleontological data are placed at ~228 mbsf (extending from 260 to >600 ka) and at 294 mbsf (extending from 900 ka to 1.2 Ma) (Stow et al., 2013). The short time interval covered between the two successive hiatuses made the correlation of the HSGR log pattern difficult, and is mainly constrained by the shipboard biostratigraphic data. The time windows of the hiatuses are tentatively refined to 280–650 ka and 750–1150 ka and are coincident with the LQD and MPD regional discontinuities identified on multichannel seismic profiles (Hernández-Molina et al., 2016). In the topmost 27 m of the Hole (last ~30 ky), as for Site U1386C, the HNGR log shows a bigradational pattern, which is interpreted as an artifact. The mean sedimentation rates vary from 29 cm/ky below the MDP to 80 cm/ky above the LQD (Fig. 6E), which is in relative agreement with the shipboard estimates (75 and 85 ky, Stow et al., 2013) for the upper interval only.

3.3. Spectral analyses

In the four studied sites, analysis reveals a well-developed cyclostratigraphic pattern in HSGR log time-series, occurring at the Milankovitch-scale frequencies with close to 100% CL significance (Fig. 8). Most of the peaks are concentrated in three frequency bands: 1) in the higher frequency band, two main peaks at 23 ky and 19 ky are common in most of the studied sites, except in Site U1386 were only the peak at 23 ky is registered; 2) in the middle frequency band, a variability of cycles are registered in the range of 55–38 ky. The 38 ky cycle is observed at both Sites U1387 and U1391; and 3) in the lower frequency band, cycles at 95–105 ky (with common records at 100 ky) are present. Isolated but significant peaks are also registered at 13 ky and 29 ky in Site U1386, and at 68–65 ky in Sites U1386 and U1387.

Cyclostratigraphic analysis provides evidence of orbital control at the Earth's orbital cycles of precession (19 ky–23 ky), obliquity (main period of 41 ky and secondary periods of around 29 ky and 54 ky) and short-term eccentricity (95 ky–123 ky) (Berger et al., 1989; Laskar et al., 1993).

4. Discussion

In this study, the GR log patterns correlate well at the regional scale over the last 1.4 My. As seen in Figs. 3, 4 and 6, the GR signal appears to be the essentially driven by the expression of the changes in the relative proportion of clay versus other non-alluminosilicate minerals, usually coarser siliciclastic or carbonate minerals. Consequently, the GR signal variability will result from a combination of several superimposed factors that can impact one or more of these three parameters: clay content, carbonate content and grain size. These factors are discussed hereafter.

4.1. GR and contourite beds

With the exception of Site U1385, bi-gradational contouritic sequences are common throughout Unit I (Stow et al., 2013; Table 1; Fig. 1). Thin turbidite intercalations were locally reported in sediment younger than ~1.45 Ma (Stow et al., 2013), but they appear to represent a minor portion of the sedimentary records and/or could be reworked by bottom currents (Takashimizu et al., 2016). Turbidites are generally more abundant at depth, in intervals not covered in this study. Thus we assume that the coarse grained Pleistocene records of the CDS are dominated by contourite beds. The bi-gradational contourite depositional sequence is classically interpreted as reflecting changes in bottom current competency and velocity (Faugères et al., 1984; Stow et al., 2008; Stow and Faugères, 2008; Rebesco et al., 2014). Coarser-grained intervals reflect phases of current intensification, generating sediment re-suspension of previously deposited material. The coarser mode thus becomes predominant while the amount of finer particles decreases due to winnowing (Faugères et al., 1984; Llave et al., 2006). For this reason, contourite deposits in the CDS of the Gulf of Cádiz form sedimentary archives that are crucial for paleoceanographic reconstructions of the MOW, possibly recording changes in flow velocity and spatial and temporal variability of its path along the Iberian margin.

Over the studied interval, the coarse-grained contourite beds are evidenced by well-expressed troughs (thin incursion to relatively low values) in the GR signal (Figs. 3 and 4). Most of the time, these drops correlate in core levels with an increase in sand fraction, and likely reflect increased MOW velocity, depleting the sediment in clay particles and enriching it in silts, sands and biogenic remains (Fig. 3). This interpretation appears to be supported by the associated increase in current velocity as evidenced by the Zr/Al core data (Figs. 3, 6). Bottom current processes are thus inferred to have dominated both sediment transport and deposition at the origin of the coarse-grained deposits in the CDS. The few coarse-grained intervals fitting with a peak in GR counts (e.g. Hole U1387A, Core 26X, orange arrows in Fig. 4) are possibly due to the presence of radioactive minerals (e.g. K feldspar), or more likely because deposition is associated with a decrease in the $CaCO_3$ content. Where some decreases in GR counts do not correlate with obvious changes in the lithological logs (blue arrows in Fig. 4), several explanations may account for these observations. Firstly, the GR drop fits with a coarse-grained interval which has not been described in the VCDs but which is revealed by grain-size analysis (e.g. Hole U1387B, Core 33 X, ~300 mbsf, blue arrow). Secondly, the GR drop reflects an increase in $CaCO_3$ content in the sediment record (Fig. 6), with no major change in grain size and thus no link with a change in bottom current velocity. Finally, some decreases in the GR counts may be artifacts possibly tying with core cracks and voids due to gas expansion, or with core section breaks, especially when they correspond to narrow and wel pronounced drops, occurring with a regular spacing of 1.5 m

Fig. 5. Regional scale correlation of the normalized HSGR downhole logs (gray shaded area) for Sites U1391, U1386, U1387, U1389 and U1390, plotted in time. The intervals in which age models were available are highlighted with a black line on the right end of the shading. The revised spliced NGR core and age model for Site U1385 is from Hodell et al. (2015). The $\delta^{18}O$ LR04 stack curve is from Lisiecki and Raymo (2005). MIS = marine isotope stage; LQD (Late Quaternary discontinuity) and MPD (mid-Pleistocene discontinuity) predicted from seismic data (Hernández-Molina et al., 2016). Vertical dotted arrows indicate interval in which change in sedimentation rate occurs. Horizontal lines indicate the main Gamma Ray horizons (GRH) identified at the regional scale. Gray boxes at the top of Holes U1386C and U1390A indicate anomalies in the log pattern reflecting acquisition artifact.

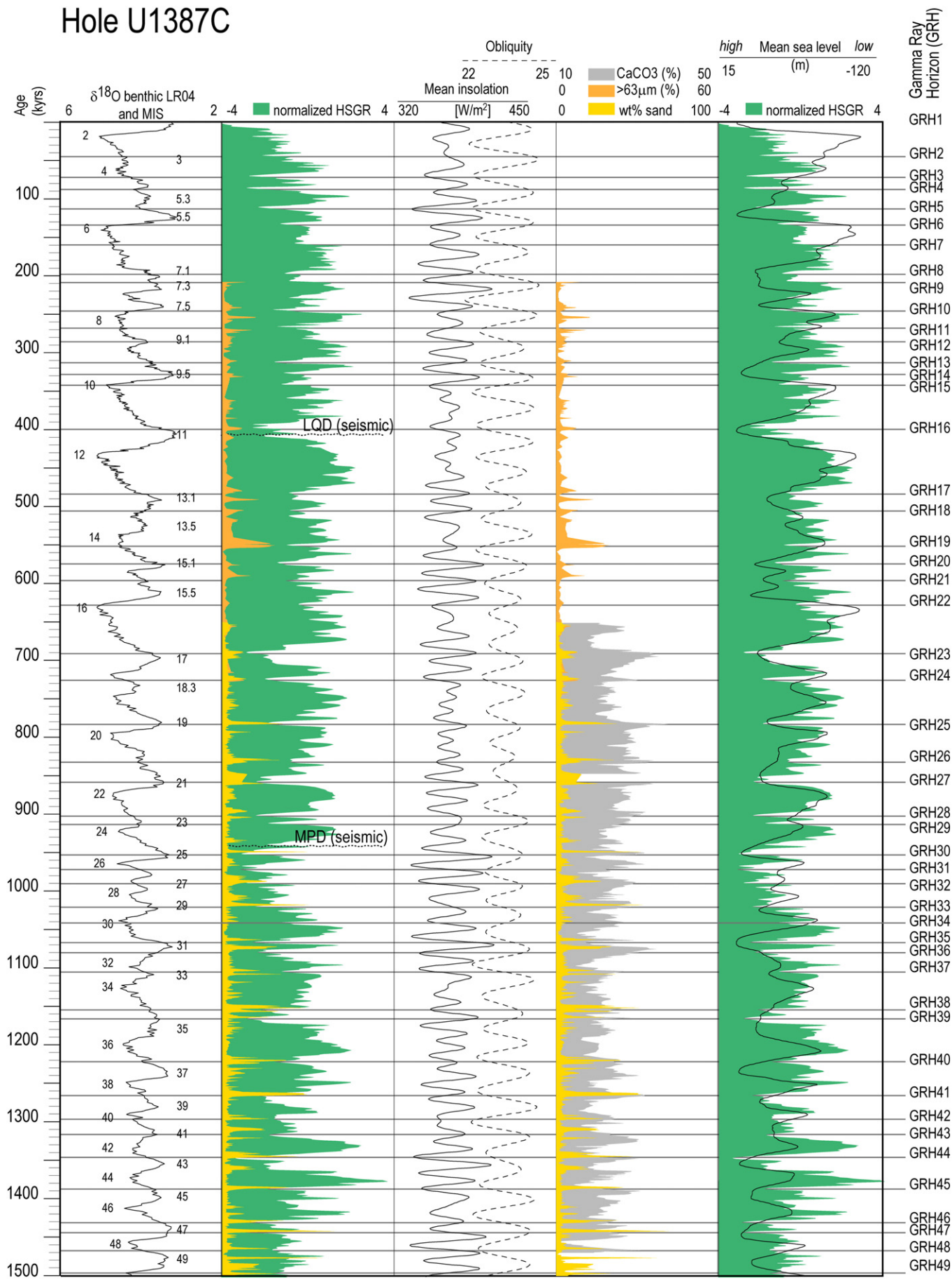
Hole U1387C
Age (kyrs)
δ18O benthic LR04 and MIS
normalized HSGR
Obliquity
Mean insolation [W/m2]
CaCO3 (%)
>63µm (%)
wt% sand
high
Mean sea level (m)
low
Gamma Ray Horizon (GRH)
LQD (seismic)
MPD (seismic)

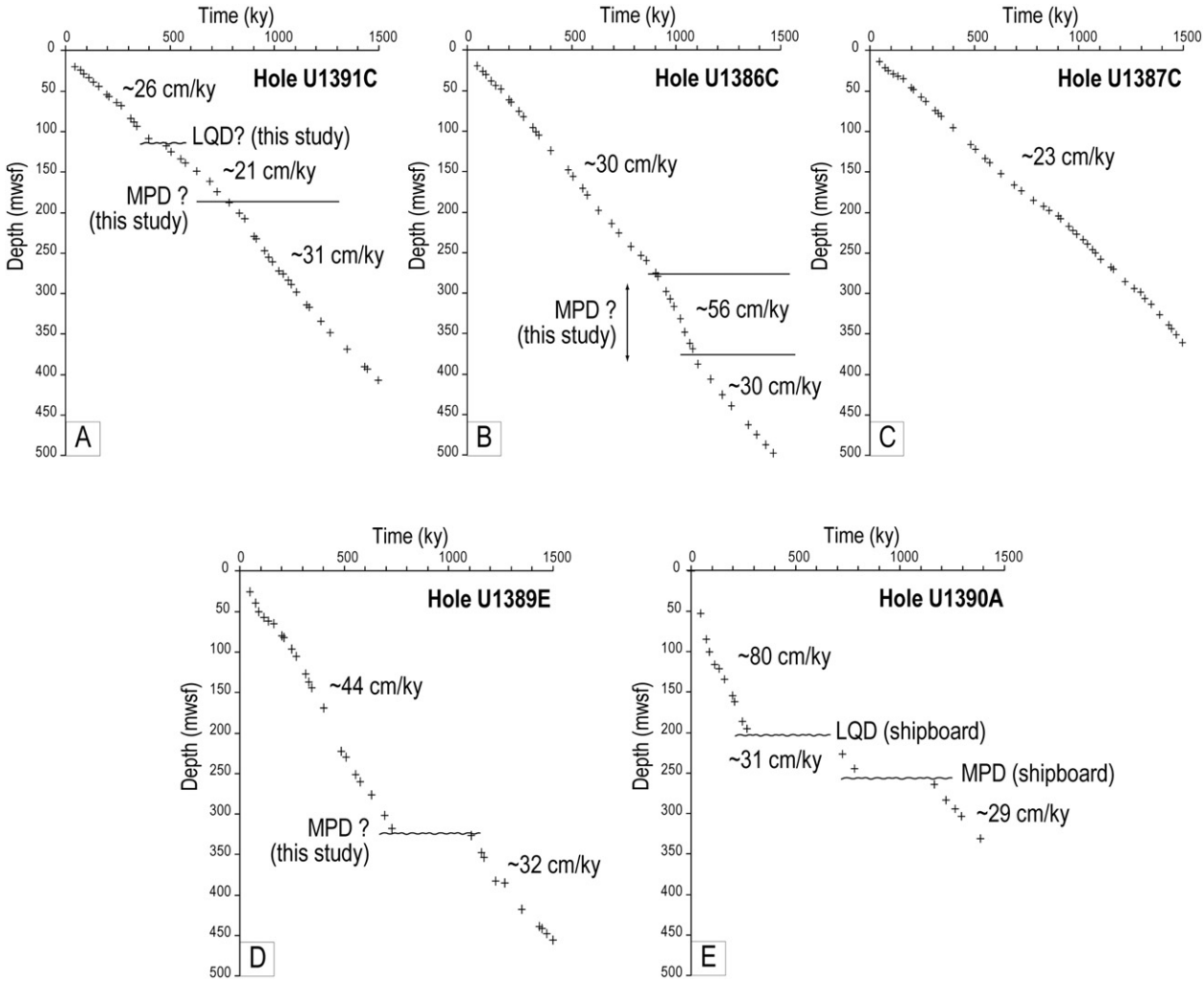

Fig. 7. Mean sedimentation rates for Holes U1391C, U1386C, U1387C, U1389E and U1390A derived from the regional scale correlation of the HSGR downhole logs. LQD: Late Quaternary discontinuity; MPD: mid-Pleistocene discontinuity.

corresponding to the core section length (e.g. Hole U1387B, Core 17X, blue arrows).

Besides some exceptions previously mentioned, the GR troughs that are superimposed on the low amplitude variability in the GR signal generally identify coarse-grained deposits, depleted in clays and enriched in carbonates (Fig. 4), and interpreted as coarse grained contourite deposits. The HSGR and NGR logs can thus be used to track and correlate some coarse-grained contourite beds across sites, at the regional scale.

4.2. Gamma Ray horizons (GRH)

In this study, we identified 49 GRH that can be traced at the regional scale in the CDS, and that are interpreted as reflecting coarse contourite deposits. Since coarser contourite layers are now thought to be formed during insolation minima and millennial-scale cold stages/oscillations (Bahr et al., 2014, 2015; Voelker et al., 2015; Lebreiro et al., 2015; Singh et al., 2015; Kaboth et al., 2016), we assume that GRH can be considered as isochronous within the studied area (Table 3). This assumption is partly supported by the relatively good correspondence in age of some GRH contained in the topmost part of Sites U1386, U1387 and U1389 (for which age models are available, Table 1). For example, the GR troughs forming GRH 6 are dated at ~133 ky at the 3 sites (U1386, U1387, U1389; Fig. 5). Past studies, however, found a slight diachronism in some contourite deposits along the Portuguese margin (Schönfeld and Zahn, 2000; Schönfeld et al., 2003). It has also been pointed out that the grain-size signal across sites may be diachronous, especially regarding relatively warm stadials such as during MIS 5 (Bahr et al., 2015). This is illustrated for example by the GR troughs forming GRH 4 and GRH 5 (respectively dated at ~87 ky and ~112 ky at Site U1387), that are slightly offset in time (older) at Sites U1386 and U1389 (see asterisk in Fig. 5). However, these offsets/diachronisms occur at the millennial or shorter scale, which is below the limit of the vertical resolution (20–30 cm) of the HSGR logs. We thus believe that, at the orbital scale, the GRH we identified within the CDS can be considered as isochronous at the orbital scale, within an uncertainty of ±10 ky (i.e., half a precessional cycle).

This interpretation is partly supported by the GR signal at Site U1385, and for which an accurate age model has been built (Table 1; Hodell et al., 2015). Contourites being absent at Site U1385, the GR signal is not expected to be identical to the ones from the CDS. The

Fig. 6. Normalized HSGR downhole logs (green), spliced sand fraction >63 μm (medium orange) and spliced weight percent (wt.%) of the sand fraction >63 μm (yellow) and carbonate content (gray)have been plotted in time for Site U1387, together with the mean insolation, obliquity, and (reversed) sea level curves. $\delta^{18}O$ LR04 stack curve is from Lisiecki and Raymo (2005); sea level curve from de Boer et al. (2014). MIS = marine isotope stage; LQD (Late Quaternary discontinuity) and MPD (mid-Pleistocene discontinuity) predicted from seismic data (Hernández-Molina et al., 2016). Horizontal lines indicate the main Gamma Ray horizons (GRH) identified at the regional scale.

general GR pattern correlates however very well across all Sites, thus supporting our interpretation (Fig. 5). Moreover, some of the GRH identified in the CDS correlate well in time with GR troughs at Site U1385 (e.g. GRH 12, 14, 16, 20, 25, 27) or fall in the vicinity of some low GR values (e.g. GRH 5, 17, 26, 28, 29, 30, 33, 44), with a temporal offset generally below 10 ky. These synchronicity/temporal offsets are discussed in Section 4.3, in the light of regional climate and oceanographic processes that determine the GR variability at the orbital scale.

4.3. GR and orbital forcing

Cyclostratigraphic analysis of the HSGR signal suggests that the sedimentation in the CDS can be considered mainly as precession and eccentricity forced, with a comparatively minor incidence of obliquity (Fig. 8). Significant cyclicity at 100 ky (and minor variations between 95 ky and 105 ky) reveals the importance of the short-term eccentricity-orbital signal for all of our sites in the Gulf of Cádiz (U1386, U1387, and U1389) or off the West Iberian margin (U1391). Obliquity is also recognized in the records but it has a comparatively weaker signal, with a higher variability and lower regularity in the registered cycles (38 to 55 ky). Sea-level changes, which are mainly driven by eccentricity in the last 900 ky and obliquity in earlier times, can explain the eccentricity and obliquity cyclicities observed in the GR in term of terrigenous input associated to coastline and river mouth shifts during sea level changes (Sierro et al., 1999). At Site U1387, the (reversed) sea level curve correlates relatively well with the general trend of the GR signal (Fig. 6), suggesting that the relative $CaCO_3$ content is diluted by an increased amount of clay supplied to the depositional area during low sea levels, and inversely. This correlation is also observed at the other sites, including U1385 (Fig. 5), but seems less clear since about ~350 ky and possibly no longer true for the last ~130 ky (Figs. 5 and 6). Times of highstands during interglacial periods tend to reduce the relative contribution of siliciclastic material to the basin, including the supply of clay, and to increase the proportion of carbonate. Coarse contourite deposits thus often correlate with peaks in carbonate content (Figs. 4 and 6). Peaks in biogenic production alone tend to provide GR drops much less pronounced than in presence of a contourite deposits. By contrast, during lowstands in glacial times the supply of siliclastic and clay sediment increases (Sierro et al., 1999) and the relative proportion of carbonate is reduced. In consequence, we can conclude that sea level is one of the main mechanisms controlling the GR variability in the Iberian margin, resulting in lowest GR levels during interglacial or highstand periods (Figs. 5 and 6). The similarities between GR patterns recorded in the contourite system of the Gulf of Cádiz and the one from Site U1385, which is well outside the contourite system, can thus be partly explained because they are all controlled by a similar sea-level change pattern. Some of the most prominent GRH are clearly related to the most prominent interglacials during the last 1.4 million years (e.g. GRH1, GRH6, GRH10, GRH16, Figs. 5 and 6).

Superimposed on this sea-level cyclicity, a well-defined precession cyclicity is also recognized by the presence of the two major cycles at 19 ky and 23 ky (Fig. 8). The significance and regularity of these peaks, independent of the site location, reflects a major incidence of precession, which results in cyclical changes of terrigenous input and/or cyclical changes in MOW velocity. Precessional cycles in sediment input have already been recognized in the sedimentary records of the western Iberian margin (Thomson et al., 2000; Hodell et al., 2013; Hodell et al., 2015) and of the continental shelf and upper slope of the Gulf of Cádiz (Sierro et al., 2000; Hernández-Molina et al., 2002). Sierro et al. (2000) for example found a prominent precessional periodicity in the Lower Pliocene records of the Gulf of Cádiz from GR log interpretation. These authors interpreted this cyclicity in terms of oscillations of annual rainfall in southern Spain, controlling the flux of clay delivered by the rivers. Cyclic changes in biogenic production may also contribute to the GR signal, although the link between changes in carbonate content and precession is not straightforward at Site U1387 (Fig. 6). We thus interpret the strong precessional periodicity in our GR log records in term of variation in clay content (relative to carbonate content) in the sediment. Since the CDS Sites are relatively close to the coastline, GR maxima reflecting clay-rich intervals likely formed under wet conditions at times of high river discharge during

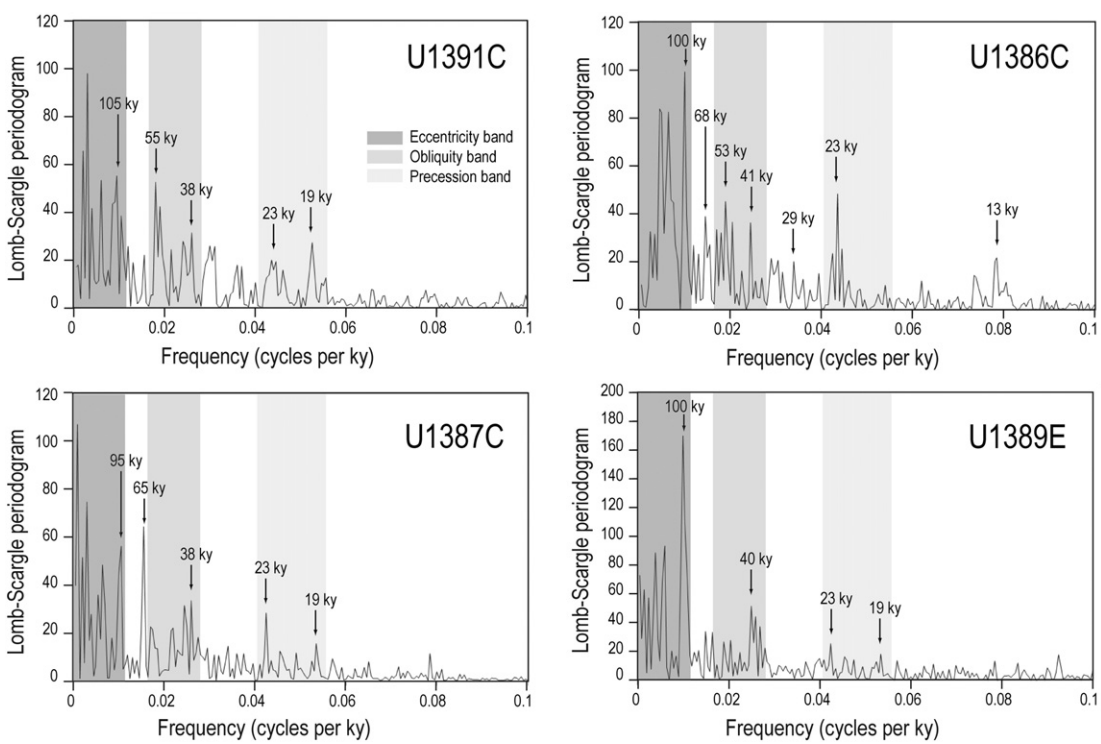

Fig. 8. Spectral analysis of the normalized HSGR logs at the studied sites. Only the peaks with a confidence level close to 100% at the permutation-test have been indicated in the power spectra. In gray the theoretical Milankovitch bands of precession, obliquity and eccentricity are indicated.

precession minima/insolation maxima (Sierro et al., 2000). Inversely, clay poor (carbonate rich) intervals emplaced during drier conditions are associated with insolation minima (Sierro et al., 2000; van der Laan et al., 2005; van der Schee et al., 2015; Voelker et al., 2015). At Site U1385, dominated by hemipelagic sedimentation, the opposite is observed and carbonate-rich intervals are preferentially emplaced during insolation maxima (Hodell et al., 2015), possibly because clays supplied by river runoff do not reach this Site. The GR response between Site 1385 and the sites drilled in the CDS are thus expected to be in opposite phase at the precession orbital scale, at least over some intervals. As an example, this opposition in phase is illustrated by GRH 4, which developed in the CDS during an insolation minimum and correlates at Site U1385 with a GR peak (increase in clay content).

Precession-driven changes in relative clay content are thus a common mechanism to all sites investigated in this work (CDS sites and Site U1385). This can explain again many of the similarities between the GR records from the different sites. However, precession-driven changes in the activity of the MOW also exert a major influence on the GR records, but this influence should be only recorded in the CDS and not in Site U1385. Independently of what was the relative supply of siliciclastic clay versus carbonate, which is driven by sea level and precession driven changes of the Iberian climate, the activity of the MOW tends to modify the GR properties of the sediments by removing the fine-grained particles from the sea floor, including clay. Enhanced MOW activity has always has a strong impact on grain size though winnowing the fine-grained particles, resulting in silty or sandy contourite beds. Its impact on the GR depends on the differential removal of clay versus other non-alluminosilicate minerals, including carbonate minerals (either fine grained or coarse grained) or coarse siliciclastic minerals. Silty or sandy contourite beds, which are the result of strong currents, are usually characterized by low contents of clay and a large proportion of sandy particles either formed by coarse carbonate shells or coarse siliciclastic material. The GR values of these beds depend on the relative contribution of these two last components that are dominated by non-alluminosilicate minerals. Besides precession-control oscillations in sediment input, GR cycles are thus also driven by precession-induced cycles in sediment grain size related to cyclical changes in the intensity of the MOW (Voelker et al., 2015; Lebreiro et al., 2015; van der Schee et al., 2015). Coarse contourite layers, which are more sandy, also form preferentially during precession maxima/insolation minima (Voelker et al., 2015; Bahr et al., 2015; Kaboth et al., 2016; Lebreiro et al., 2015). This relationship is illustrated in Fig. 6, in which the spliced coarse grained fraction has been plotted in time for Site U1387, together with the mean insolation curve. Although not all of them, several of the GR lows, interpreted as reflecting coarse contourite beds (see Section 4.2 below), correlate with insolation minima. GR thus tends to be high at times of insolation maxima because of the high input of clay and/or because of the low removal of clay from the sediments due to the lesser activity of the MOW during these times. By contrast, GR is low at times of insolation minima because of the lower supply of clay (higher carbonate) and the preferential winnowing of clay that result in a sandy or silty contourite bed. The MOW flow signal (via grain sorting/winnowing) thus appears concomitantly superimposed to the clay supply signal, both mechanisms acting in phase. However, while the MOW flow signal is thought to be driven by changes of the Mediterranean climate, clay supply reflects climate changes in Southern Spain and Portugal (Sierro et al., 2000). Obviously, unlike the other effects, the cyclical changes associated to variations in MOW strength should not be recorded at Site U1385, assuming that this Site was not affected by the MOW during the last million years.

The GR record in the CDS thus appears to be essentially driven by glacioeustatic fluctuations (mainly controlled by obliquity) and precession related climatic changes. Both are probably impacting the amount of terrigenous clay supplied to the sea from the continent. The good correlation between the general trend of the GR curves acquired in the CDS and the GR data from Site U1385, drilled out of the MOW path and dominated by hemipelagic sedimentation, apparently support this interpretation that the supply of clay material and sea level play an important role in the GR variability (Fig. 5). Precession-driven changes in Iberian climate drive cyclical changes in sediment input to the basin while precession-driven changes in Mediterranean exert a strong influence on the GR records by altering the patterns of particle removal via grain sorting/winnowing. It is to note that, as shown in Fig. 6, some of the GR lows (fitting with coarse grained layers) at Site U1387 also correlate with obliquity maxima or decreasing phase (e.g. GRH 25, 30, 35, 47), suggesting that there could be some obliquity influence on the activity of the MOW (in speed and/or depth).

4.4. Vertical variability of the MOW

Keeping in mind the temporal scale at which they can be considered as isochronous, the GRH horizons reflect coarse contourite deposits in the CDS (Fig. 6) and correlate well at the regional scale, independently of the site location (Fig. 5). Moreover, many of these GRH correlate with periods of high sea levels (e.g. MIS 5–25, 35–39, 43–47 in Figs. 5 and 6) suggesting that coarser contourites at the studied sites are preferentially formed during interglacial periods (in this paper we use the term “interglacial” in the broader sense of glacial/interglacial cycles and not restricted to the true interglacial sub-stage such as MIS 5e, 11c, and 19c). The spliced coarse-grained fraction from Site U1387 over the interval extending between GRH 8 and GRH 49 nicely illustrates this correlation (e.g. GRH 25 and MIS 19, Fig. 6). Conversely, high GR values (clay-rich intervals) usually correlate with periods of low sea levels at glacial times. MIS 12, 16 and 22 for example appear as well expressed expanded clay-rich intervals (Fig. 5), associated with glacial periods.

In addition to the sea-level signal, within longer lasting interglacial MIS, some GR minima of lower amplitude can be observed, showing a pronounced astronomical cyclicity (precession) and corresponding to contourites deposited at times of summer insolation minima under the action of an intensified MOW flow (Voelker et al., 2014; Lebreiro et al., 2015; Bahr et al., 2015; Kaboth et al., 2016). This includes the Holocene when contourites, independently of their location beneath the path of the upper or lower MOW core (Llave et al., 2006; Voelker et al., 2006; Toucanne et al., 2007; Bahr et al., 2014), were formed at the beginning of the insolation minimum. The observed GR/precession relationship seems to apply also to interstadials occurring during some glacial stages such as during MIS 10 and 16 (Figs. 5 and 6). This behavior is classically related with cyclical changes in intensity of the MOW driven by changes in Mediterranean Sea climate (Voelker et al., 2015; Singh et al., 2015; Bahr et al., 2015; Kaboth et al., 2016). This pattern is however better expressed at interglacial times, supporting the interpretation that contourites at the studied sites are preferentially formed during warm climate periods. At a shorter time scale, some contourites are also deposited during millennial-scale cold stages/oscillations (Voelker et al., 2006, 2015; Llave et al., 2006; Toucanne et al., 2007; Bahr et al., 2014, 2015; Kaboth et al., 2016).

Our observations thus suggest that, besides being deposited at times of summer insolation minima, coarse-grained contourite deposits over the study area also seem to have preferentially been emplaced during interglacial periods, as a result of increased bottom current velocity (Figs. 3, 6). Conversely, with few exceptions (e.g. MIS 14, Fig. 6), coarse contourite deposits are rare during glacial periods, as a result of decreased bottom current velocity. This is especially clear for MIS 12 and 16 that are associated with expanded clay-rich intervals in which essentially fine grained contourites can be observed (e.g. ~650 ky in MIS 16; Fig. 6). This correlation to the sea-level appears to be independent of the site location, beneath the present day path of the upper or lower MOW core. At first view, our observations could suggest an intensification of the MOW flow at interglacial times compared to glacial times, which should be in contradiction with the idea of a denser and faster MOW during cold periods (e.g. Rogerson et al., 2005; Llave et al., 2006). Indeed, cold climatic intervals are thought to be favorable

to deep-sea water formation in the Mediterranean Sea and associated increase in the MOW density and thus intensity (e.g. Cacho et al., 2000; Rogerson et al., 2012). An enhanced Mediterranean circulation during Heinrich event 1 and last Glacial Maximum conditions in comparison to warmer intervals has for example been proposed by Cacho et al. (2000) based on a study performed in the Alboran sea and by Toucanne et al. (2012) for mid-depth levels along the Corsica margin. It is thus probable that our observations more likely reflect changes in depth position of the MOW between glacial and interglacial times, as already observed over the last cycles. Indeed, based on benthic foraminiferal assemblage studies on the Portuguese margin, Schönfeld and Zahn (2000) and Schönfeld et al. (2003) proposed that during the last Glacial, the MOW was flowing about 700 m deeper than today. The GR log from Site U1391, drilled in the same area, clearly shows that the coarser contourite beds were emplaced preferentially during interglacial periods (Fig. 5). However, Site U1391 is located at a water depth of ~1073 m, thus shallower than the depth at which the MOW was flowing during the last glacial maximum according to Schönfeld and Zahn (2000) (1600–2000 mbsl). Thus, although Site U1391 is presently located under the lower core of the MOW path, contourite deposition at this site appears essentially driven by the upper branch of the MOW, during both warm and cool periods. It is thus expected that if the lower core of the MOW was enhanced and flowing deeper during glacial periods, associated contourite beds should have been emplaced at water levels exceeding the depth of Site U1391, i.e. deeper than ~1100 mbsl, which is in agreement with what has been proposed by Schönfeld and Zahn (2000) and Hernández-Molina et al. (2014b). Regarding the Gulf of Cádiz, Sites U1386 and U1387 were drilled under the path of the present day upper MOW core and present a behavior similar to Sites U1391 and U1389, which are drilled on the path of the present day lower MOW core. Site U1390 has been drilled at a water depth of 990 mbsl. The Pleistocene at this site is not continuous due to the presence of two hiatuses, and the GR log pattern is consequently not very clear. However, over the last ~280 ky, the log pattern between GRH 4 and GRH 12 is relatively similar to the one of Site U1389, drilled in the vicinity at a shallower water depth (~645 mbsl). Sedimentation at Site U1390 thus could also be influenced by the upper branch of the MOW, during at least some periods such as the GR4–GR12 interval (i.e. ~87–280 ka). Similarly to the observations made on the Portuguese margin, if the MOW was enhanced during glacial periods, it was probably flowing deeper than the depth of Site U1390 (990 mbsl), at least during some periods.

During most of the glacial periods, the studied CDS sites were thus under the action of a MOW flow which was weakened compared to interglacial periods. At the same time, a stronger and denser flow is thought to be flowing at greater water depths (e.g. Rogerson et al., 2005). Here, we propose an additional mechanism which, combined with the variability in flow density and vertical glacial/interglacial position of the MOW, could account for our observations. Indeed, several studies demonstrated that high suspended-sediment concentrations deeply modify the dynamic structure of a flow. With an increase in clay concentration, a flow can thus be transformed from turbulent to laminar (e.g. Baas et al., 2009). We consequently suggest that the large amount of clay supplied from the rivers during glacial periods may have impacted the MOW flow behavior and competence, and contributed to weaken the flow, especially in its upper core which is close to the source of sediment supply. Inversely, during highstands, as the clay supplied from the rivers is mainly stored at shallow water depths, the turbulence and real competence of the MOW is not expected to be affected.

4.5. Hiatuses

We propose that the site to site correlation of the GR logs acquired in the CDS contains a regional record of the interglacial MOW flow and its orbital scale variability. None of the drilled sites provides evidence for strong glacial MOW flow under the form of coarse contourites, which is consistent with the work of Schönfeld and Zahn (2000). Hernández-Molina et al. (2014b) also stressed that the present-day flow of the MOW is mainly as the upper core along the upper slope and the proximal part of the middle slope. A denser, deeper and enhanced circulation of the MOW as the lower core is inferred during climatically cold intervals. In this interpretation, we should expect the presence of deep water glacial contourite drifts, especially along western Iberia. This should be the case of some drifts found along the Galicia Margin, which are deeper than the drifts in the Gulf of Cádiz (Ercilla et al., 2008, 2010, 2011; Mena et al., 2010; Hernández-Molina et al., 2011). Hernández-Molina et al. (2014a,b, 2016) also suggest that the downward displacement of the MOW, coupled with significant intensification of MOW current activity, can explain the formation of the largest hiatuses observed in the CDS at 3.2 to 3.0 Ma, 2.4 to 2 Ma and at 0.9 to 0.7 Ma (MPD). These periods would be coeval with global coolings, sea-level falls, and enhanced thermohaline circulation and AMOC. These events also coincide with pronounced changes in the sedimentary stacking pattern observed in the CDS (Llave et al., 2001, 2007; Roque et al., 2012; Marchès et al., 2010). Among these hiatuses, one falls in the time window covered by our studied interval: the MPD, possibly coinciding with the middle Pleistocene transition (Lisiecki and Raymo, 2005), during which the climate system evolved from the 41 ky to the 100 ky world (Imbrie et al., 1992; Clark et al., 2006). Above the MPD, the LQD unconformity is dated at ~0.4 Ma (Hernández-Molina et al., 2016). Fig. 5 shows the location of the LQD and MPD hiatuses, either inferred from seismic profile interpretation (Hernández-Molina et al., 2016), evidenced by Exp. 339 biostratigraphic data (Site U1390, Stow et al., 2013), or proposed in this study. Hernández-Molina et al. (2016) report that these hiatuses are related to discontinuities, which represents angular erosional unconformities on the basin margins and the flanks of the topographic highs, changing laterally to concordance in the middle of the basins. Therefore, the time interval for the hiatus is laterally variable, since the amount of sediment eroded by the bottom-current increases toward topographic highs, where the unconformity would represent a much longer hiatus. Some of these hiatuses coincide with changes in estimated sedimentation rates at the drilling sites (see also Fig. 7). The first one (LQD) falls into the MIS 12–11 interval and corresponds to a condensed section at Site U1385 (Hodell et al., 2015), a possible hiatus at site U1391 (this study), a hiatus at Site U1390 and to the LQD seismic unconformity observed in the same time window, or close to it at Sites U1386, U1387 and U1389 (Llave et al., 2001, 2007; Roque et al., 2012; Hernández-Molina et al., 2016) (Fig. 5). Despite the absence of evidence in the HSGR logs supporting the presence of a seismic unconformity at Sites U1386, U1387 and U1389, we propose that if the LQD results from an intensification of the MOW, it could have occurred at ~410–420 ka at most of the studied sites (Fig. 5), lasting to ~240 ky at Site U1390. The second expected unconformity (MPD) has been clearly identified at Site U1390 where it corresponds to a ~ 400 ky long hiatus (Stow et al., 2013), which age is tentatively refined to 0.75–1.15 Ma. Based on GR correlation patterns, we propose that this hiatus is also present at Site U1389, with an ~350 ky duration (0.75–1.1 Ma). The existence of the MPD unconformity is less clear at the other Sites from GR data. It may correspond with changes in sedimentation rates at Site U1391 between 0.78 and 0.86 Ma, close to the MDP seismic unconformity which is observed in the same time window, and at Site U1386 between ~0.95 and 1.15 Ma (Figs. 6 and 7). The strong erosional character of the MPD at Sites U1389 and U1390 compared to the others may reflect the vicinity of the Strait of Gibraltar (stronger flow), although the importance of the slope morphology in the location of the hiatuses must not be neglected (Hernández-Molina et al., 2016).

5. Summary and conclusions

Until IODP Exp. 339, knowledge of the CDS in the Gulf of Cádiz and on the West Iberian margin mainly relied on seismic profile interpretation

and on ^{14}C dated sediment core data covering the last 50 ky. The direct cause–effect link between climate, MOW, and CDS is not yet fully understood, but cold climatic intervals are thought to be favorable to deep-sea water formation in Mediterranean Sea and associated increase in the MOW density and intensity (Rogerson et al., 2012; Cacho et al., 2000). These CDS have been recently drilled in several places during IODP Exp. 339, accessing the internal Pliocene and Quaternary architecture of the system, and allowing the observations done on recent deposits to be tested over Quaternary sedimentary history.

In the present study, we use downhole and core GR data acquired from 5 sites drilled in the CDS (U1386, U1387, U1389 and U1391), and one site (U1385) drilled in a deeper setting, out of the MOW path. The GR log patterns in the CDS are characterized by medium-amplitude cyclic swings correlating well across the sites over the last 1.4 My. The GR data are essentially driven by changes in the relative proportion of clay versus other non-alluminosilicate minerals, usually coarser siliciclastic or carbonate minerals. The GR signal variability results from a combination of several superimposed orbitally forced mechanisms that can impact clay content, carbonate content and grain size.

- Mechanism 1 corresponds to sea level changes as supported by the well expressed eccentricity and obliquity cyclicities evidenced from cyclostratigraphic analysis performed on the GR data. This mechanism results in an increased clay content supplied by the rivers during glacial periods and acts on all the Sites drilled in the CDS as well as Site U1385.
- Mechanism 2 corresponds to precession-driven climate changes over the Iberian Peninsula, at the origin of increased clay content during wet climatic conditions (insolation maxima/precession minima). This mechanism is superimposed to mechanism 1 and acts especially in the sites drilled in the CDS since they are relatively close to the coastline.
- Mechanism 3 corresponds to precession-driven changes in Mediterranean climate and hydrologic budget which impact the MOW's density. Sandy contourite beds are the expression of the bottom current processes and are evidenced by pronounced drops in GR values. They are often preferentially emplaced during drier climatic conditions (insolation minima/precession maxima). This mechanism, only acting on the Sites drilled in the CDS, is concomitant with mechanism 2 and superimposed to mechanism 1.

This study also suggests that, besides being deposited at times of summer insolation minima, some of the contourite beds are preferentially emplaced during interglacial periods and could be obliquity driven. Oppositely, coarse contourite deposits are rare during glacial periods, which is consistent with the hypothesis of an enhanced glacial MOW flowing at greater water depths, out of the study area, during Quaternary sea-level low stands. We further suggest that during glacial periods, the large amount of clay supplied by the rivers may also have impacted the MOW flow behavior and competence, and contributed to weaken the flow, especially in its upper core.

We identified several GRH (well expressed drops in the GR logs) that can be confidently traced across the 5 studied sites and that are interpreted as reflecting coarse contourite deposits. In this study, we consider the GRH as isochronous at the orbital scale, within an uncertainty of ~±10 ky. We propose that the GRH can be used in the CDS as a regional scale stratigraphic tool. Studies depicting the large-scale picture of the CDS essentially rely on seismic profile interpretations. With appropriate time-depth conversion law, GRH tied to seismic lines could allow refinement of the internal architecture of the CDS with a high accuracy. This is especially true for drifts that are bounded laterally by erosional channels (e.g. Site U1389) making regional correlations of the seismic reflectors difficult. GR horizons could further allow testing the origin of some of the cyclic patterns observed in the seismic records (Llave et al., 2001, 2007). For example, the strong 5th order precession signal in the GR data of the CDS could possibly be at the origin of these patterns. GRH can also be used to show the presence of hiatuses and changes in sedimentation rates that may reflect some period of MOW intensification. We thus suggest the presence of an ~350 ky long hiatus (0.75–1.1 Ma) at Site U1389, probably related to a major regional seismic discontinuity (MPD) marking a pronounced change in the drift sedimentary stacking pattern and indicating an intensification of the MOW (Hernández-Molina et al., 2016). The LQD regional seismic unconformity dated at ~0.4 Ma (Hernández-Molina et al., 2016) is observed in the MIS 11–12 interval and tentatively refined to ~410–420 ky.

This study confirms that the vertical displacement of the MOW and possibly the percentage of clay input in the Gulf of Cádiz and along the West Iberian margin between glacial and interglacial times, appear to play an important role in the pattern of bottom current behavior and the contourite deposition. The characteristic GR patterns can be used to address this spatio-temporal variability, as well as for regional correlation and dating in CDS. Past studies have already pointed out that GR logs can be used for high-resolution bed-to-bed astrochronological correlations (Sierro et al., 2000). This approach still needs to be tested on other CDS, in order to address the impact on the GR signal of the climate, oceanographic and sedimentary processes variability that determine CDS growth.

Acknowledgments

This research used data and samples provided by the Integrated Ocean Drilling Program (IODP). A.V. acknowledges funding by the Fundação para a Ciência e a Tecnologia (FCT; Portugal) through the MOWCADYN project (PTDC/MAR-PRO/3761/2012) and a FCT Investigador contract. This contribution is partially supported through the CTM 2008-06399-C04/MAR (CONTOURIBER), CTM 2012-39599-C03 (MOWER), CGL2011-26493, SA263U14, as well as the Continental Margins Research Group (CMRG) at Royal Holloway University of London (UK). E.D. thanks the INSU post-campagne program and Action Marges (INSU) for financial support. We thank Dr. D. Van Rooij and an anonymous reviewer for helpful reviews.

References

Alonso, B., Ercilla, G., Stow, D.A.V., Hernández-Molina, F.J., Llave, E., 2016. Contourite vs gravity-flow deposits of the Faro Drift (Gulf of Cadiz) during the Pleistocene: sedimentological and mineralogical approaches. Mar. Geol. 377, 77–94.

Baas, J.H., Best, J.L., Peakall, J., Wang, M., 2009. A phase diagram for turbulent, transitional, and laminar clay suspension flows. J. Sediment. Res. 79, 162–183.

Bahr, A., Jimenez Espejo, F.J., Kolasinac, N., Grunert, P., Hernández-Molina, F., Röhl, U., Voelker, A., Escutia, C., Stow, D.A.V., Hodell, D., Alvarez Zarikian, C.A., 2014. Deciphering bottom current velocity and paleoclimate signals from contourite deposits in the Gulf of Cádiz during the last 140 kyr: an inorganic geochemical approach. Geochem. Geophys. Geosyst. 15 (8), 3145–3160.

Bahr, A., Kaboth, S., Jimenez Espejo, F.J., Sierro, F.J., Voelker, A.H.L., Lourens, L., Roehl, U., Reichart, G.J., Escutia, C., Hernández-Molina, F.J., Pross, J., Friedrich, O., 2015. Persistent monsoonal forcing of Mediterranean Outflow dynamics during the late Pleistocene. Geology 43, 951–954.

Baringer, M.O., Price, J.F., 1999. A review of the physical oceanography of the Mediterranean outflow. Mar. Geol. 155, 63–82.

Berger, A.L., Loutre, M.F., Dehant, V., 1989. Milankovitch frequencies for pre-Quaternary. Nature 342, 133.

Borenäs, K.M., Wåhlin, A.K., Ambar, I., Serra, N., 2002. The Mediterranean outflow splitting—a comparison between theoretical models and CANIGO data. Deep-Sea Res. II Top. Stud. Oceanogr. http://dx.doi.org/10.1016/S0967-0645(02)00150-9.

Brackenridge, R.E., Hernández-Molina, F.J., Stow, D.A.V., Llave, E., 2013. A Pliocene mixed contourite–turbidite system offshore the Algarve Margin, Gulf of Cadiz: seismic response, margin evolution and reservoir implications. Mar. Pet. Geol. 46, 36–50.

Cacho, I., Grimalt, J.O., Sierro, F.J., Shackleton, N., Canals, M., 2000. Evidence for enhanced Mediterranean thermohaline circulation during rapid climatic coolings. Earth Planet. Sci. Lett. 183 (3–4), 417–429.

Clark, P.U., Archer, D., Pollard, D., Blum, J.D., Rial, J.A., Brovkin, V., Mix, A.C., Pisias, N.G., Roy, M., 2006. The middle Pleistocene transition: characteristics, mechanisms, and implications for long-term changes in atmospheric pCO_2. Quat. Sci. Rev. 25 (23–24), 3150–3184.

de Boer, B., Lourens, L.J., van de Wal, R.S.W., 2014. Persistent 400,000 year variability of Antarctic ice volume and the carbon cycle is revealed throughout the Plio-Pleistocene. Nat. Commun. 5.

Ducassou, E., Fournier, L., Sierro, F.J., Alvarez Zarikian, C.A., Lofi, J., Flores, J.A., Roque, C., 2016. Origin of the large Pliocene and Pleistocene debris flows on the Algarve margin. Mar. Geol. 377, 58–76.

Ellis, D.V., Singer, J.M., 2007. Well Logging for Earth Scientists. second ed. Springer, Dordrecht, Netherlands (692 pp.).

Ercilla, G., García-Gil, S., Estrada, F., Gràcia, E., Vizcaino, A., Vázquez, T., Díaz, S., Vilas, F., Casas, D., Alonso, B., Dañobeitia, J., Farran, M., 2008. High resolution seismic stratigraphy of the Galicia Bank Region and neighbouring abyssal plains (NW Iberian continental margin). Mar. Geol. 249, 108–112.

Ercilla, G., Casas, D., Iglesias, J., Vázquez, J.T., Somoza, L., León, R., Medialdea, T., Juan, C., García, M., 2010. Contourites in the Galicia Bank region (NW Iberian Atlantic). Geo-Temas 11, 33–34.

Ercilla, G., Casas, D., Vázquez, J.T., Iglesias, J., Somoza, L., Juan, C., Medialdea, T., León, R., Estrada, F., García-Gil, S., Farran, M., Bohoyo, F., García, M., Maestro, A., ERGAP Project and Cruise Teams, 2011. Imaging the recent sediment dynamics of the Galicia Bank region (Atlantic, NW Iberian Peninsula). Mar. Geophys. Res. 32 (1–2), 99–126.

Faugères, J.-C., Gonthier, E., Stow, D.A.V., 1984. Contourite drift molded by deep Mediterranean outflow. Geology 12, 296–300.

Faugères, J.-C., Frappa, M., Gonthier, E., de Resseguier, A., Stow, D.A.V., 1985. Modelé et facies de type contourite à la surface d'une ride sédimentaire édifiée par des courants issus de la veine d'eau méditerranéenne (ride du Faro, Golfe de Cadix). Bull. Soc. Geol. Fr. 1 (1), 35–47.

García, M., Hernández-Molina, F.J., Llave, E., Stow, D.A.V., León, R., Fernández-Puga, M.C., Díaz del Río, V., Somoza, L., 2009. Contourite erosive features caused by the Mediterranean Outflow Water in the Gulf of Cádiz: Quaternary tectonic and oceanographic implications. Mar. Geol. 257 (1–4), 24–40.

Gonthier, E.G., Faugères, J.C., Stow, D.A.V., 1984. Contourite facies of the Faro Drift, Gulf of Cádiz In: Stow, D.A.V., Piper, D.J.W. (Eds.), Fine-grained Sediments: Deep Water Processes and Facies. Geological Society Special Publications 15, pp. 275–292.

Hanquiez, V., Mulder, T., Lecroart, P., Gonthier, E., Marchès, E., Voisset, M., 2007. High resolution seafloor images in the Gulf of Cádiz, Iberian margin. Mar. Geol. 246 (1), 42–59.

Hernández-Molina, F.J., Somoza, L., Vazquez, J.T., Lobo, F., Fernández-Puga, M.C., Llave, E., Díaz-del Río, V., 2002. Quaternary stratigraphic stacking patterns on the continental shelves of the southern Iberian Peninsula: their relationship with global climate and palaeoceanographic changes. Quat. Int. 92 (1), 5–23.

Hernández-Molina, J., Llave, E., Somoza, L., Fernández-Puga, M.C., Maestro, A., León, R., Medialdea, T., Barnolas, A., García, M., Díaz del Río, V., Fernández-Salas, L.M., Vázquez, J.T., Lobo, F., Alveirinho Dias, J.M., Rodero, J., Gardner, J., 2003. Looking for clues to paleoceanographic imprints: a diagnosis of the Gulf of Cádiz contourite depositional systems. Geology 31 (1), 19–22.

Hernández-Molina, F.J., Llave, E., Stow, D.A.V., García, M., Somoza, L., Vázquez, J.T., Lobo, F.J., Maestro, A., Díaz del Río, V., León, R., Medialdea, T., Gardner, J., 2006. The contourite depositional system of the Gulf of Cádiz: a sedimentary model related to the bottom current activity of the Mediterranean Outflow Water and its interaction with the continental margin. Deep-Sea Res. II 53 (11–13), 1420–1463.

Hernández-Molina, F.J., Serra, N., Stow, D.A.V., Llave, E., Ercilla, G., Van Rooij, D., 2011. Along-slope oceanographic processes and sedimentary products around the Iberian margin. Geo-Mar. Lett. 31 (5–6), 315–341.

Hernández-Molina, F.J., Stow, D.A.V., Alvarez-Zarikian, C.A., Acton, G., Bahr, A., Balestra, B., Ducassou, E., Flood, R., Flores, J.-A., Furota, S., Grunert, P., Hodell, D., Jimenez-Espejo, F., Kim, J.K., Krissek, L., Kuroda, J., Li, B., Llave, E., Lofi, J., Lourens, L., Miller, M., Nanayama, F., Nishida, N., Richter, C., Roque, C., Pereira, H., Sanchez Goñi, M.F., Sierro, F.J., Singh, A.D., Sloss, C., Takashimizu, Y., Tzanova, A., Voelker, A., Williams, T., Xuan, C., 2014a. Onset of Mediterranean outflow into the North Atlantic. Science 344 (6189), 1244–1250.

Hernández-Molina, F.J., Llave, E., Preu, B., Ercilla, G., Fontan, A., Bruno, M., Serra, N., Gomiz, J.J., Brackenridge, R.E., Sierro, F.J., Stow, D.A.V., García, M., Juan, C., Sandoval, N., Arnaiz, A., 2014b. Contourite processes associated with the Mediterranean Outflow Water after its exit from the Strait of Gibraltar: global and conceptual implications. Geology 42 (3), 227–230.

Hernández-Molina, F.J., Sierro, F.J., Llave, E., Roque, C., Stow, D.A.V., Williams, T., Lofi, J., Van der Schee, M., Arnaíz, A., Ledesma, S., Rosales, C., Rodríguez-Tovar, F.J., Pardo-Igúzquiza, E., Brackenridge, R.E., 2016. Evolution of the Gulf of Cádiz Margin and southwest Portugal contourite depositional system: tectonic, sedimentary and paleoceanographic implications from IODP Expedition 339. Mar. Geol. 377, 7–39.

Hodell, D., Crowhurst, S., Skinner, L., Tzedakis, P.C., Margari, V., Channell, J.E.T., Kamenov, G., Maclachlan, S., Rothwell, G., 2013. Response of Iberian Margin sediments to orbital and suborbital forcing over the past 420 ka. Paleoceanography 28, 185–199.

Hodell, D., Lourens, L., Crowhurst, S., Konijnendijk, T., Tjallingii, R., Jiménez-Espejo, F., Skinner, L., Tzedakis, P.C., Abrantes, F., Acton, G.D., Alvarez Zarikian, C.A., Bahr, A., Balestra, B., Barranco, E.L., Carrara, G., Ducassou, E., Flood, R.D., Flores, J.-A., Furota, S., Grimalt, J., Grunert, P., Hernández-Molina, J., Kim, J.K., Krissek, L.A., Kuroda, J., Li, B., Lofi, J., Margari, V., Martrat, B., Miller, M.D., Nanayama, F., Nishida, N., Richter, C., Rodrigues, T., Rodríguez-Tovar, F.J., Roque, A.C.F., Sanchez Goñi, M.F., Sierro Sánchez, F.J., Singh, A.D., Sloss, C.R., Stow, D.A.V., Takashimizu, Y., Tzanova, A., Voelker, A., Xuan, C., Williams, T., 2015. A reference time scale for Site U1385 (Shackleton Site) on the Iberian Margin. Glob. Planet. Chang. 133, 49–64.

Imbrie, J., Berger, A., Boyle, E.A., Clemens, S.C., Duffy, A., Howard, W.R., Kukla, G., Kutzbach, J.E., Martinson, B., Morley, J.J., Peterson, L.C., Pisias, N.G., Prell, W.L., Raymo, M.E., Shackleton, N.J., Toggweiler, J.R., 1992. On the structure and origin of major glaciation cycles 1. Linear responses to Milankovitch forcing. Paleoceanography 7 (6), 701–738.

Inwood, J., Lofi, J., Davies, S., Basile, C., Bjerrum, C., Mountain, G., Proust, J.N., Otsuka, H., Valppu, H., 2013. Log-based statistical classification of lithology: IODP Exp 313. Geosphere 9, 1025–1043.

Itturino, G., Liu, T., Goldberg, D., Anderson, L., Evans, H., Fehr, A., Guerin, G., Inwood, J., Lofi, J., Malinverno, A., Morgan, S., Mrozewski, S., Slagle, A., Williams, T., 2013. Performance evaluation of the current IODP wireline heave compensation system. Sci. Drill. J. 15, 46–50.

Jiménez-Espejo, F.J., García-Alix, A., Jiménez-Moreno, G., Rodrigo-Gámiz, M., Anderson, R.S., Rodríguez-Tovar, F.J., Martínez-Ruiz, F., Giralt, S., Delgado Huertas, A., Pardo-Igúzquiza, E., 2014. Saharan aeolian input and effective humidity variations over western Europe during the Holocene from a high altitude record. Chem. Geol. 374-375, 1–12.

Jiménez-Moreno, G., Aziz, H.A., Rodríguez-Tovar, F.J., Pardo-Igúzquiza, E., Suc, J.P., 2007. Palynological evidence for astronomical forcing in Early Miocene lacustrine deposits from Rubielos de Mora Basin (NE Spain). Palaeogeogr. Palaeoclimatol. Palaeoecol. 252, 601–616.

Kaboth, S., Bahr, A., Reichart, G.-J., Jacobs, B., Lourens, L.J., 2016. New insights into upper MOW variability over the last 150 kyr from IODP 339 site U1386 in the Gulf of Cadiz. Mar. Geol. 377, 136–145.

Khélifi, N., Sarnthein, M., Andersen, N., Blanz, T., Frank, M., Garbe-Schönberg Haley, B.A., Stumf, R., Einelt, M., 2011. A major and long-term Pliocene intensification of the Mediterranean outflow, 3.5–3.3 Ma ago. Geology 37, 811–814.

Khélifi, N., Sarnthein, M., Frank, M., Andersen, N., Garbe-Schönberg, D., 2014. Late Pliocene variations of the Mediterranean outflow. Mar. Geol. 357, 182–194.

Laskar, J., Joutel, F., Boudin, F., 1993. Orbital, precessional and insolation quantities for the Earth from −20 Myr to +10 Myr. Astron. Astrophys. 270, 522–533.

Lebreiro, S.M., Antón, L., Reguera, I., Fernández, M., Conde, E., Ana, I., Barrado, Y.A., 2015. Zooming into the Mediterranean Outflow moat during the 1.2–1.8 million years period (Mid-Pleistocene) — an approach by stable and radiogenic isotopes. Glob. Planet. Chang. (in press).

Lisiecki, L.E., Raymo, M.E., 2005. A Pliocene–Pleistocene stack of 57 globally distributed benthic $\delta^{18}O$ records. Paleoceanography 20, PA1003.

Llave, E., Hernández-Molina, F.J., Somoza, L., Díaz del Río, V., Stow, D.A.V., Maestro, A., Alveirinho Dias, J.M., 2001. Seismic stacking pattern of the Faro–Albufeira contourite system (Gulf of Cádiz): a Quaternary record of paleoceanographic and tectonic influences. Mar. Geophys. Res. 22 (5–6), 487–508.

Llave, E., Flores, J.A., Hernández-Molina, F.J., Sierro, F.J., Somoza, L., Díaz-del-Río, V., Martínez del Olmo, W., 2004. Cronoestratigrafía de los depósitos contorníticos del talud continental del Golfo de Cádiz a partir del análisis de nanofósiles calcáreos. Geotemas 6 (5), 183–186.

Llave, E., Schönfeld, J., Hernández-Molina, F.J., Mulder, T., Somoza, L., Diaz del Rio, V., Sanchez-Almazo, I., 2006. High-resolution stratigraphy of the Mediterranean outflow contourite system in the Gulf of Cadiz during the late Pleistocene: the impact of Heinrich events. Mar. Geol. 227 (3–4), 241–262.

Llave, E., Hernández-Molina, F.J., Somoza, L., Stow, D.A.V., Díaz Del Río, V., 2007. Quaternary evolution of the contourite depositional system in the Gulf of Cádiz. Geological Society Special Publication 276, pp. 49–79.

Llave, E., Matias, H., Hernández-Molina, F.J., Ercilla, G., Stow, D.A.V., Medialdea, T., 2011. Pliocene–Quaternary contourites along the northern Gulf of Cadiz margin: sedimentary stacking pattern and distribution. Geo-Mar. Lett. 31 (5/6), 377–390. http://dx.doi.org/10.1007/s00367-011-0241-3.

Lomb, N.R., 1976. Least-squares frequency analysis of unequally spaced data. Astrophys. Space Sci. 39, 447–462.

Maldonado, A., Nelson, C.H., 1999. Interaction of tectonic and depositional processes that control the evolution of the Iberian gulf of Cadiz margin. Mar. Geol. 155, 217–242.

Marchès, E., Mulder, T., Cremer, M., Bonnel, C., Hanquiez, V., Gonthier, E., Lecroart, P., 2007. Contourite drift construction influenced by capture of Mediterranean Outflow Water deep-sea current by the Portimão submarine canyon (Gulf of Cádiz, South Portugal). Mar. Geol. 242 (4), 247–260.

Marchès, E., Mulder, T., Gonthier, E., Cremer, M., Hanquiez, V., Garlan, T., Lecroart, P., 2010. Perched lobe formation in the Gulf of Cadiz: interactions between gravity processes and contour currents (Algarve margin, Southern Portugal). Sediment. Geol. 229, 81–94.

Margari, V., Skinner, L.C., Tzedakis, P.C., Ganopolski, A., Vautravers, M., Shackleton, N.J., 2010. The nature of millennial-scale climate variability during the past two glacial periods. Nat. Geosci. 3 (2), 127–131.

Mena, A., Francés, G., Pérez-Arlucea, M., Hanebuth, T.J.J., Nombela, M.A., 2010. Sedimentary evolution of the Galicia Inner Basin during the last 70 kyr. Geo-Temas 11, 125–126.

Millot, C., Candela, J., Fuda, J.-L., Tber, Y., 2006. Large warming and salinification of the Mediterranean outflow due to changes in its composition. Deep-Sea Res. I 53, 656–666.

Nelson, C.H., Baraza, J., Maldonado, A., Rodero, J., Escutia, C., Barber Jr., J.H., 1999. Influence of the Atlantic inflow and Mediterranean outflow currents on late Quarternary sedimentary facies of Gulf of Cádiz continental margin. Mar. Geol. 155 (1–2), 99–129.

Paillard, D., Labeyrie, L., Yiou, P., 1996. Macintosh Program performs time-series analysis. Eos. Trans. AGU 77 (39), 379.

Pardo-Igúzquiza, E., Rodríguez-Tovar, F.J., 2000. The permutation test as a non-parametric method for testing the statistical significance of power spectrum estimation in cyclostratigraphic research. Earth Planet. Sci. Lett. 181, 175–189.

Pardo-Igúzquiza, E., Rodríguez-Tovar, F.J., 2012. Spectral and cross-spectral analysis of uneven time series with the smoothed Lomb–Scargle periodogram and Monte Carlo evaluation of statistical significance. Comput. Geol. 49, 207–216.

Press, H.W., Teukolsky, S.A., Vetterling, W.T., Flannery, B.P., 1992. Numerical Recipes in Fortran. second ed. Cambridge University Press, New York, p. 963.

Rebesco, M., Hernández, M.J., van Rooij, D., Wåhlin, A., 2014. Contourites and associated sediments controlled by deep-water circulation processes: state-of-the-art and future considerations. Mar. Geol. 352, 111–154.

Rodríguez-Tovar, F.J., Reolid, M., Pardo-Igúzquiza, E., 2010. Planktonic versus benthic foraminifera response to Milankovitch forcing (Late Jurassic, Betic Cordillera): testing methods for cyclostratigraphic analysis. Facies 56, 459–470.

Rogerson, M., Rohling, E.J., Weaver, P.P.E., Murray, J.W., 2005. Glacial to interglacial changes in the settling depth of the Mediterranean Outflow plume. Paleoceanography 20, PA3007.

Rogerson, M., Rohling, E.J., Bigg, G.R., Ramirez, J., 2012. Paleoceanography of the Atlantic–Mediterranean exchange: overview and first quantitative assessment of climatic forcing. Rev. Geophys. 50, RG2003.

Roque, C., Duarte, H., Terrinha, P., Valadares, V., Noiva, J., Cachão, M., Ferreira, J., Legoinha, P., Zitellini, N., 2012. Pliocene and Quaternary depositional model of the Algarve margin contourite drifts (Gulf of Cadiz, SW Iberia): seismic architecture, tectonic control and paleoceanographic insights. Mar. Geol. 303–306, 42–62.

Scargle, J.D., 1982. Studies in astronomical time series analysis. II. Statistical aspects of spectral analysis of unevenly spaced data. Astrophys. J. 263, 835–853.

Schönfeld, J., Zahn, R., 2000. Late glacial to Holocene history of the Mediterranean Outflow. Evidence from benthic foraminiferal assemblages and stable isotopes at the Portuguese margin. Palaeogeogr. Palaeoclimatol. Palaeoecol. 159 (1–2), 85–111.

Schönfeld, J., Zahn, R., Abreu, L., 2003. Surface and deep water response to rapid climate changes at the Western Iberian Margin. Glob. Planet. Chang. 36, 237–264.

Serra, O., 1984. Fundamentals of Well-log Interpretation. Elsevier, Amsterdam, The Netherlands, p. 423.

Serra, N., Ambar, I., Käse, R.H., 2005. Observations and numerical modelling of the Mediterranean outflow splitting and eddy generation. Deep-Sea Res. II 52, 383–408.

Sierro, F.J., Flores, J.A., Baraza, J., 1999. Late glacial to recent paleoenvironmental changes in the Gulf of Cadiz and formation of sandy contourite layers. Mar. Geol. 155, 157–172.

Sierro, F.J., Ledesma, S., Flores, J.-A., Torrescusa, S., Martínez del Olmo, W., 2000. Sonic and gamma-ray astrochronology: cycle to cycle calibration of Atlantic climatic to Mediterranean sapropels and astronomical oscillations. Geology 28 (8), 695–698.

Singh, A.D., Rai, A.K., Tiwari, M., Naidu, P.D., Verma, K., Chaturvedi, M., Niyogi, A., Pandey, M.D., 2015. Fluctuations of the Mediterranean Outflow Water circulation in the Gulf of Cadiz during the MIS 5 to 7: evidences from benthic foraminiferal assemblage and stable isotope records. Glob. Planet. Chang. 133, 125–140.

Skinner, L.C., Elderfield, H., 2007. Rapid fluctuations in the deep North Atlantic heat budget during the last glacial period. Paleoceanography 22, PA1205.

Stow, D.A.V., Faugères, J.-C., 2008. Contourite facies and the facies model. In: Rebesco, M., Camerlenghi, A. (Eds.), Developments in Sedimentology. Elsevier, pp. 223–256.

Stow, D.A.V., Faugères, J.-C., Gonthier, E., 1986. Facies distribution and textural variation in Faro Drift contourites: velocity fluctuation and drift growth. Mar. Geol. 72 (1–2), 71–100.

Stow, D.A.V., Hunter, S., Wilkinson, D., Hernández-Molina, F.J., 2008. The nature of contourite deposition. In: Rebesco, M., Camerlenghi, A. (Eds.), Developments in Sedimentology. Elsevier, pp. 143–156 (Chapter 9).

Stow, D.A.V., Hernández-Molina, F.J., Alvarez Zarikian, C.A., the Expedition 339 Scientists, 2013. Proceedings IODP, 339. Integrated Ocean Drilling Program Management International, Tokyo http://dx.doi.org/10.2204/iodp.proc.339.2013.

Takashimizu, Y., Kawamura, R., Rodríguez-Tovar, F.J., Dorador, J., Ducassou, E., Hernández-Molina, F.J., Stow, D.A.V., Alvarez-Zarikian, C., 2016. Reworked tsunami deposits by bottom current: evidences from Late Pleistocene to Early Holocene in the Gulf of Cádiz. Mar. Geol. 377, 95–109.

Thomson, J., Nixon, S., Summerhayes, C.P., Rohling, E.J., Schonfeld, J., Zahn, R., Grootes, P., Abrantes, F., Gaspar, L., Vaqueiro, S., 2000. Enhanced productivity on the Iberian margin during glacial/interglacial transitions revealed by barium and diatoms. J. Geol. Soc. 157, 667–677.

Toucanne, S., Mulder, T., Schoenfeld, J., Hanquiez, V., Gonthier, E., Duprat, J., Cremer, M., Zaragosi, S., 2007. Contourites of the Gulf of Cadiz: a high-resolution record of the paleocirculation of the Mediterranean outflow water during the last 50,000 years. Palaeogeogr. Palaeoclimatol. Palaeoecol. 246 (2–4), 354–366.

Toucanne, S., Jouet, G., Ducassou, E., Bassetti, M.-A., Dennielou, B., Angue Minto'o, C.M., Lahmi, M., Touyet, N., Charlier, K., Lericolais, G., Mulder, T., 2012. A 130,000-year record of Levantine Intermediate Water flow variability in the Corsica Trough, western Mediterranean Sea. Quat. Sci. Rev. 33, 55–73.

van Aken, H.M., 2000. The hydrography of the mid-latitude Northeast Atlantic Ocean — part I: the deep water masses. Deep-Sea Res. I 47, 757–788.

van der Laan, E., Gaboardi, S., Hilgen, F.J., Lourens, L.J., 2005. Regional climate and glacial control on high-resolution oxygen isotope records from Ain el Beida (latest Miocene, NW Morocco): a cyclostratigraphic analysis in the depth and time domain. Paleoceanography 20 (1), PA000995.

Van der Schee, M., Sierro, F.J., Flecker, R., Gutjahr, M., Jimenez-Espejo, F.J., Hernández-Molina, F.J., Grunert, P., Garcia Gallardo, A., Flores, J.A., Hodell, D., Andersen, N., 2015. Discussion on identification of the Mio-Pliocene boundary and onset of the MOW recorded in IODP Site U1387C in the Gulf of Cádiz. RCMNS Interim Colloquium, Mediterranean–Atlantic Gateway (Neogene to present) (Rabat (Morocco), 5–8 May, 2015. Abstract volume).

Voelker, A.H.L., Lebreiro, S.M., Schönfeld, J., Cacho, I., Erlenkeuser, H., Abrantes, F., 2006. Mediterranean Outflow strengthening during Northern Hemisphere coolings: a salt source for the glacial Atlantic? Earth Planet. Sci. Lett. 245 (1–2), 39–55.

Voelker, A.H.L., Jimenez-Espejo, F.J., Bahr, A., Acton, G.D., Rebotim, A., Salgueiro, E., Röhl, U., Escutia, C., 2014. Mediterranean Outflow Water changes in the Gulf of Cadiz during the Mid-Pleistocene transition — the role of insolation. In: van Rooij, D., Rüggeberg, A. (Eds.), Book of Abstracts. 2nd Deep-Water Circulation Congress: The Contourite Log-book. Ghent, Belgium, 10–12 September 2014VLIZ Special Publication 69. Ghent University, Department of Geology and Soil Science — Flanders Marine Institute (VLIZ), Oostende, Belgium, pp. 29–30.

Voelker, A.H.L., Salgueiro, E., Rodrigues, T., Jiminez-Espejo, F.J., Bahr, A., Alberto, A., Loureiro, I., Padilha, M., Rebotim, A., Röhl, U., 2015. Mediterranean outflow and surface water variability off southern Portugal during the early Pleistocene: a snapshot at marine isotope stages 29 to 34 (1020–1135 ka). Glob. Planet. Chang. 133, 223–237.